

## A Spectroscopic Search for High Mass X-ray Binaries in M31

B. F. Williams<sup>1</sup>, D. Hatzidimitriou<sup>2</sup>, J. Green<sup>3</sup>, G. Vasilopoulos<sup>4</sup>, R. Covarrubias<sup>5</sup>, W.N. Pietsch<sup>4</sup>, H. Stiele<sup>6</sup>, F. Haberl<sup>4</sup>, P. Bonfimi<sup>7</sup>

### ABSTRACT

We present new optical spectroscopy of 20 candidate counterparts of 17 X-ray sources in the direction of the M31 disc. By comparing the X-ray catalogue from the XMM-Newton survey of M31 with star catalogues from the Local Group Galaxy Survey, we chose counterpart candidates based on optical colour and X-ray hardness. We have discovered 17 counterpart candidates with spectra containing stellar features. Eight of these are early-type stars of O or B type in M31, with hard X-ray spectra, making them good HMXB candidates. Three of these eight exhibit emission lines, which we consider to be the strongest HMXB candidates. In addition, our spectra reveal two likely Galactic cataclysmic variables, one foreground M star, two probable LMXBs related to M31 globular clusters, one emission line region with an embedded Wolf-Rayet star, and one newly-discovered supernova remnant. Finally, two of the sources have stellar spectra with no features indicative of association with an X-ray source.

*Subject headings:* galaxies: individual (M31) — X-ray binaries — galaxies: spiral

### 1. Introduction

One puzzling mystery surrounding our neighboring spiral galaxy M31 is that while the Milky Way, which is comparable in mass and morphology, has 130 known high-mass X-ray binaries (HMXBs), M31 has none. Galactic high-mass X-ray binaries (HMXBs) typically contain stars of spectral type O8–B3 (Liu et al. 2000). These stars have  $-5 < M_V < -2$ , or  $19.7 < V < 22.7$

---

<sup>1</sup>Department of Astronomy, Box 351580, University of Washington, Seattle, WA 98195

<sup>2</sup>University of Athens, Faculty of Physics, Department of Astrophysics, Astronomy and Mechanics, Panepistimiopolis, GR15784 Zografos, Athens, Greece

<sup>3</sup>Center for Astrophysics, 60 Garden Street, Cambridge, MA 06540

<sup>4</sup>Max-Planck-Institut für extraterrestrische Physik, 85741 Garching, Germany

<sup>5</sup>National Optical Astronomy Observatories, Colina El Pino, Casilla 603 La Serena, Chile

<sup>6</sup>Shanghai Astronomical Observatory, 80 Nandan Road, Shanghai 200030 China

<sup>7</sup>Centre for Astrophysics and Supercomputing, Mail number H30 Swinburne University of Technology, PO Box 218, Hawthorn, Victoria 3122, Australia

when scaled to the distance of (780 kpc; Holland et al. 1996; McConnachie et al. 2005) and reddening ( $A_V = 0.3$  Dalcanton et al. 2012) of M31. We have performed a spectral survey of bright blue optical counterpart candidates of catalogued X-ray sources in an attempt to discover the HMXB population of M31, and to begin measuring its characteristics.

Being young objects, HMXBs are associated with star formation. In M31, star formation is mostly associated with the disc. An investigation of the star formation rate of the disc has been conducted by Williams (2003), who finds that the mean SFR over the last 60 Myr for  $1.4 \text{ deg}^2$  of the M31 disc is  $0.63 \pm 0.07 M_\odot \text{ yr}^{-1}$  (in the range  $0.1\text{-}100 M_\odot$ ) with no drastic changes. We used the calibration of Grimm et al. (2003) to calculate the expected number of HMXBs (see comment in Shtykovskiy & Gilfanov 2005, regarding the normalization) to be  $\simeq 2$  HMXBs brighter than  $10^{38} \text{ erg s}^{-1}$ , and  $\simeq 32$  sources brighter than  $10^{36} \text{ erg s}^{-1}$ .

Alternatively, recent work on the luminosity function of HMXBs in the Small Magellanic Cloud has resulted in a different shape than for larger galaxies (Sturm et al. 2013). While this shape may not be relevant for the larger galaxy M31, it is more sharply cut off at luminosities  $>10^{36} \text{ erg s}^{-1}$ . Scaling the SMC HMXB XLF by a factor of 6 to account for the higher star formation rate in M31, we would expect  $\simeq 40$  HMXBs with a luminosity above  $10^{36} \text{ erg s}^{-1}$ , but none brighter than  $10^{37} \text{ erg s}^{-1}$ .

The estimates are reasonable, given that the Galaxy has  $\simeq 20$  HMXBs with X-ray luminosities  $>10^{36} \text{ erg s}^{-1}$  (Grimm et al. 2002), which could be detected at the distance of M31. However, HMXBs are difficult to find at that distance, as evidenced by the fact that M33, at similar distance and star formation rate but with lower star density and dust content, has just 3 known HMXBs (Long et al. 2002; Pietsch et al. 2006, 2009), one of which has been confirmed with radial velocities (Orosz et al. 2007).

M31 has been well-observed and catalogued in the X-ray and optical (Williams et al. 2004; Pietsch et al. 2005; Stiele et al. 2011; Massey et al. 2006; Dalcanton et al. 2012), so one would expect that HMXBs would have been discovered and confirmed by now, as is the case with M33; however, there are several possible reasons why we have not yet found any confirmed HMXBs in M31. The most likely is that they are more heavily crowded by other stars and more heavily reddened than in M33. Another possibility is that the relatively low star formation rate, and high metallicity (solar–supersolar; Zaritsky et al. 1994) may hamper HMXB production (Dray 2006). Another possibility is that many of the HMXBs in M31 are too faint to be detected by our currently-available surveys.

While deep *Chandra* observations of M31 are mainly limited to the central portions of the galaxy (Kaaret 2002; Williams et al. 2006; Voss & Gilfanov 2007; Garcia et al. 2010; Barnard et al. 2013; Hofmann et al. 2013), where spectroscopic follow-up is very difficult, XMM-Newton has surveyed the entire galaxy (Stiele et al. 2011). XMM-Newton EPIC observations taken between June 2006 and February 2008, together with archival observations (Pietsch et al. 2005) from June 2000 to July 2004 yielded a total of 1948 X-ray sources (0.2–12.0 keV) covering (for the first time) the

entire D25 ellipse of M 31, down to a limiting luminosity of  $\simeq 10^{35}$  erg s $^{-1}$  in the 0.2-4.5 keV band (Stiele et al. 2011). These sources include (i) sources within M31, i.e. X-ray binaries, supernova remnants (SNRs) and supersoft sources, (ii) foreground (Galactic) stars and (iii) background objects, i.e. mostly active galactic nuclei, some normal galaxies and a few clusters of galaxies. Hardness ratios, X-ray variability and correlations with catalogues in other wavelengths (optical, radio) have been used in an attempt to classify the various X-ray sources. However, a high percentage (65%) of the sources can still only be classified as <hard> sources, i.e. it is not possible to determine whether these sources are X-ray binaries or Crab-like SNRs in M31, or background X-ray sources (mainly AGNs) not associated with M31.

Here, we discuss spectroscopic results regarding the X-ray binary population revealed by these X-ray data and follow-up optical spectroscopic observations of counterpart candidates found within these data sets, including 8 bright, early-type stars that are probable HMXBs. Two of these 8 have spectra with emission lines, making them good HMXB candidates. Another one of these 8 has a spectrum similar to Be stars, making it a strong Be-HMXB candidate. Many of the other spectra obtained were newly-discovered AGN behind M31 which will be discussed in another paper (Green et al., in prep.). Section 2 describes how our counterpart candidates were selected, the data acquisition and reduction process, and the classification of the optical spectra. Section 3 details our results, providing descriptions of each HMXB candidate individually, and Section 4 summarizes our findings.

## 2. Data

### 2.1. Counterpart Selection

Optical counterparts of the X-ray sources were sought within the optical catalogue of M31 from the Local Group Galaxy Survey (LGGS Massey et al. 2006), which provides stellar photometry covering the entire optical disc of M31. The photometric accuracy is 1% down to 21st magnitude, and the positional accuracy is 0.25". We cross-correlated the Pietsch et al. (2005) and Massey et al. (2006) catalogues, using a  $3\sigma$  (combined X-ray and optical positional uncertainty) search radius. Typical search radii were  $\simeq 4''$ , and the local densities of bright blue stars in the Massey et al. (2006) catalogue within  $0.1^\circ$  of our spectroscopy targets was  $\leq 6$  arcmin $^{-2}$ , making the chance superposition rate  $\leq 8\%$ .

The optical counterparts of HMXBs are expected to be Be stars or supergiants. Using the V-band magnitude and colour limits for Be stars from (Sabogal et al. 2005), and taking into account the distance modulus and interstellar absorption of M31, we have estimated blue supergiants and Be stars in M31 to have apparent magnitudes in the range  $V = 17 - 25$  and  $-0.4 < B - V < 0.8$ , with the bright end ( $V < 19.5$ ) being supergiants and the faint end ( $V > 19.5$ ) being Be stars. Among the optical counterparts of X-ray sources mentioned above, down to the limiting magnitude of 20.5 (where the Massey et al. 2006 is highly complete), there are 91 objects within the expected colour

range. However, with our available telescope and instrument (described below), we were able to obtain spectra for  $\sim 6$  objects per season. Since about half of the observed sources turned out not to be stellar, our final stellar sample for this work was 20 spectra of 17 objects in the 7 season campaign.

## 2.2. Optical observations

The optical data presented here were acquired with the 3.5m telescope at the Apache Point Observatory (APO), located in the Sacramento Mountains in Sunspot, New Mexico (USA). Observations were carried out during fall of 2006, 2008 and 2011, during summer and fall of 2007, 2009, fall of 2011 and summer of 2012.

The telescope was equipped with the Dual Imaging Spectrograph (DIS), a medium dispersion spectrograph with separate collimators for the red and blue part of the spectrum and two 2048x1028 E2V CCD cameras, with the transition wavelength around 5350Å. For the blue branch, a 400 lines/mm grating was used, while the red branch was equipped with a 300 lines/mm grating. The nominal dispersions were 1.83Å/pixel and 2.31Å/pixel, respectively, with central wavelengths at 4500Å and 7500Å. The nominal wavelength coverage provided by this instrument setup around the central value was 4660Å and 7620Å for the two branches, respectively. However, due to vignetting towards the chip edges, the wavelength regions actually used were somewhat reduced (blue: 3750 - 5400Å, red: 5200 - 8000Å). A 1.5" slit was employed.

Exposure times ranged from 900 to 2700 s, depending on the magnitude of the object, as well as on seeing and weather conditions. At least three exposures were obtained per object; some of the targets required 4 or 5 exposures. Each on-target series of exposures was followed by a comparison lamp exposure (HeNeAr) for wavelength calibration. Spectra of two spectrophotometric flux standards (Feige110 and BD+28-4211) were acquired during the same observing runs. A series of 22 spectroscopic standards of mainly early spectral types were also observed.

Figure 1 shows the location of the observed sources (red symbols) on an optical unfiltered image of M31 obtained with the Schmidt telescope on Calar Alto (using HDAP which was produced at Landessternwarte Heidelberg-Königstuhl under grant No. 00.071.2005 of the Klaus-Tschira-Foundation). On the same plot we have marked with cyan the locations of OB stars in M31 (obtained using appropriate colour and magnitude cuts from the Massey et al. 2006 catalogue), which delineate the spiral arms. The vast majority of the objects were observed both in blue and red, usually with the same total exposure time.

A total of 20 objects' (non-AGN) spectra have been acquired, as likely counterparts of 17 X-ray sources. 16 of the spectra obtained have coverage from 3750-8000 Å, the others have only 3750-5200 Å because the red detector was not functioning from November 2006 to September 2007. The details of the observations of stellar spectra are reported in Table 1, the X-ray properties of the objects, including positional offsets, are in Table 2, while the LGGS optical photometry data

and 2MASS IR photometry data for the counterparts observed are given in Table 3. The other spectra will be described in a paper detailing the AGN (J. Green et al., in prep.). The structure of the Table 1 is as follows:

1. *Column 1* gives the Massey et al. (2006) catalogue number
2. *Column 2* gives the X-ray source number of the target as it appears in PFH2005.
3. *Column 3* lists the Right Ascension of the optical counterparts (epoch 2000).
4. *Column 4* gives the Declination of the optical counterparts (epoch 2000)
5. *Column 5* gives the date of the observation at APO telescope.
6. *Column 6* shows whether the target was observed in the blue (B) or red (R) channel
7. *Column 7* lists the total exposure time for the specific spectrum
8. *Column 8* provides the number of individual exposures acquired for the corresponding spectrum.

Finally, we also observed a set of early-type stars with known spectral types, given in Table 4, for use in cross-correlation tests to quantify our qualitative classifications where possible.

### 2.3. Data reduction

The data reduction was performed with the *NOAO-IRAF* FITS Image Kernel (July 2003), using standard procedures: First, the frames were bias-subtracted and flat-fielded. The 2-D spectra were subsequently traced and extracted using the all-in-one package *apextract*. Comparison lamp spectra were then extracted from the corresponding lamp exposures, using the profiles measured for the corresponding object spectra. The comparison lamp spectra were used to provide the wavelength calibration of the object spectra. The resulting accuracy of the wavelength calibration is  $\sim 1\text{\AA}$  (see §2.2 for spectral resolution). Flux calibration was achieved using the spectrophotometric flux standard spectra. The spectrophotometric standard spectra were processed with the same tools as the object spectra. Then the fluxes as a function of wavelength were compared to the published values from Massey et al. (2006) to produce a sensitivity map, which was then applied to all of our observed spectra. The calibrated object spectra were combined, weighting according to exposure time, to yield the final spectrum. This reduction and calibration procedure was also adopted to the spectroscopic standards.

## 2.4. Spectral Classification

A first level of classification of the observed spectra was performed by visual inspection. The original set of spectra obtained, included several cases of active galactic nuclei (AGN), showing characteristic, usually broad, emission lines. These will be discussed in a separate publication (J. Green et al., in prep.). The rest of the spectra were either stellar or nebular (SNRs or HII regions) or a combination of the two. Spectra showing a strong continuum with relatively narrow, or lack of, absorption and/or emission lines, were classified as stellar. If a spectrum showed strong  $H\alpha$  and [S II] emission lines, it was classified as a SNR or an HII region, depending on the relative strengths of these lines. Blue stellar spectra were roughly classified by eye and put through the IRAF cross-correlation routine `fxcor` against our set of spectral standards in Table 4, which returns a peak cross-correlation strength and best-fit velocity.

## 3. Results

After initial classifications into Star, AGN, or SNR/HII region, we had 20 stellar spectra, or stellar spectra combined with diffuse emission, corresponding to 17 X-ray sources, out of spectra of counterpart candidates of 41 X-ray sources. Sources [PMH 224], [Steile 235], and [PMH 367] each have 2 counterpart candidates for which we obtained spectroscopy.

The optical and X-ray brightness distribution of the stars, compared to the overall distribution of our sample is shown in Figure 2. We then determined which of these stars were in M31 using their velocities. Any star showing an emission or absorption line feature corresponding with a blue shift corresponding to the velocity of M31 was considered a M31 member. Of the 20 spectra considered here, 2 are foreground objects (LGGs J004123.75+411459.6, LGGs J004445.06+415153.4), 5 are unlikely to be the correct counterpart (LGGs J003937.27+404928.9, LGGs J004216.78+404814.4, LGGs J004259.07+413731.4, LGGs J004456.78+413548.0, LGGs J004604.83+415142.4), two are different parts of the same SNR in M31 (LGGs J004210.24+405149.4, LGGs J004210.38+405148.1). Two are star clusters in M31 (LGGs J004218.72+411401.2, LGGs J004309.86+411900.9) The other 9 are stars in M31.

Any star in M31 with luminosities meeting our selection criteria that is a member of M31 ( $V < 20.5$ ;  $M_V < -4$  at the distance of M31) associated with an X-ray source with a hard spectrum should be considered a good HMXB candidate; however, relatively red spectra could be low-mass stars in the late stages of stellar evolution. Furthermore, stellar spectra showing no atypical features (e.g., emission lines), may be chance superpositions with the X-ray source error circle. Therefore, our best HMXB candidates are those that are the bluest and show atypical spectral features for single stars. There are 11 X-ray sources with a counterpart candidate spectrum of a star in M31, 9 of these 11 have spectral types that only apply to stars with masses  $\gtrsim 5 M_\odot$  (one is a WN star, 8 are HMXB candidates), and 3 of these 9 have spectral features that may indicate interaction with an X-ray-emitting companion (*i.e.*, emission lines). We discuss all of the spectra in detail below.

### 3.1. [PFH2005] 136 – Galactic Dwarf Nova

The only optical counterpart within the positional error-circle of this X-ray source down to the LGGS (Massey et al. 2006) limiting magnitude, is the peculiar variable R066 (Rosino 1973, their object R066=R081). This object is known to show repeated optical outbursts, and has been classified by Rosino as either a recurrent nova in M31, or, more likely a U GEM variable (dwarf nova from accreting white dwarf Tovmasyan 1984) in our Galaxy. Sharov & Alksnis (1989) pointed out that a U GEM variable classification would be consistent with the short interval between outbursts (recurrent novae flare up more rarely) and the very high rate of decrease in brightness following an outburst. The object is also given a U Gem-variable “uncertain” classification in the Catalogue of Cataclysmic Variables of Downes et al. (2001, online edition updated in 2006), in the General Catalogue of variable stars (as M31-V0609; Samus et al. 2009), and in the AAVSO International Variable Star Index VSX (Watson et al. 2013).

The blue stellar spectrum we obtained for R066 (Figure 3) shows clear Balmer line emission ( $H_\beta$ ,  $H_\gamma$ ,  $H_\delta$  and  $H_\epsilon$ ) with a velocity of  $+70 \text{ km s}^{-1}$ . The red stellar spectrum (Figure 4) is consistent with an M5/M6 dwarf in our Galaxy, with prominent TiO bands (6322Å, 6569Å, 6651Å, 7053Å, 7666Å, 8206Å, 8432Å). The classification of the star as a dwarf is based on the strength of the near infrared sodium doublet (Na 8183/8195Å), which is a sensitive gravity indicator (Schiavon et al. 1997). The 2-MASS infrared colours ( $J - H = 0.47 \pm 0.09$ ,  $H - K = 0.45 \pm 0.10$ ) are also consistent with this classification. Indeed, at quiescence, U Gem variables (dwarf novae) are characterized by a strong Balmer emission spectrum on a blue continuum, while in the infrared, in relatively long orbital period systems, the spectrum of the secondary dominates. The secondary in U-Gem’s is very often a mid M dwarf, as is the case here (e.g. Warner 1995).

Most bright dwarf novae at quiescence have been detected in hard X-rays (0.1-5 keV), while soft X-rays (100-200 eV) have been detected in quiescence in very few systems (e.g. Warner 1995). Thus, both optical and X-ray properties of source [PFH2005] 136 are consistent with it being a dwarf nova in the Galaxy.

### 3.2. [PFH2005] 146 – M31 WR and O Star Bubble?

Within the 2.5-sigma error circle (3.65 arcsec radius) of the X-ray position, there are 5 candidate optical counterparts in the Massey catalogue. We have obtained a spectrum of the brightest and bluest counterpart, LGGS\_J004130.37+410500.9. The others are separated by  $>1''$ , and are fainter, so that they are unlikely to have significantly affected the spectrum of LGGS\_J004130.37+410500.9.

The X-ray source [PFH2005] 146 is spatially correlated with a catalogued HII region in M31 (Baade & Arp 1964; Pellet et al. 1978; Kraemer et al. 2002). The object is also recorded in the radio in Braun (1990). PFH2005 have classified it as an SNR, on the basis of its hardness ratios and the presence of radio emission. The LGGS object we observed is catalogued as an  $H\alpha$  emission

line object in Massey et al. 2006 who have classified it as a Wolf-Rayet star of WNL type embedded in an HII region, on the basis of a low resolution spectrum.

Our spectrum of LGGJ004130.37+410500.9 is very similar to the spectrum of NGC604-WR12 in M33 of type WN, in Drissen et al. (2008). It appears to be a composite spectrum of a WR star and an HII region. In Figures 5 and 6, we label parts of the spectrum with the characteristic lines of HII regions and WR stars identified in different colours.

### 3.2.1. HII- region component

Table 5 presents a summary of the most significant nebular emission lines identified in the spectrum of the object [PFH2005] 146. We report the rest frame wavelengths and the observed ones, as well as the fluxes derived using the deblending/fitting function provided by the *IRAF* task *noao.onedspec.splot*.

The blueshift of the lines is  $\Delta\lambda \simeq 10\text{\AA}$ , which yields an approximate radial velocity of  $RV \sim -450 \text{ km s}^{-1}$ , thus confirming M31 membership.

The line ratios of characteristic lines are compatible with an HII region. SNR shocks are expected to create strong  $[SII] \lambda\lambda 6716, 6731$  emission lines, typically with  $[SII]/H\alpha > 0.4 - 0.5$  - empirical criterion value (see for example Matonick & Fesen 1997, and references therein). Referring to Table 5, for object [PFH2005] 146 this ratio is about 0.29. Furthermore, the relative fluxes  $[SII](6731 + 6716)/H\alpha$  and  $[OIII](5007)/H\beta$  for the the object data are well within the HII region boundary of Kewley et al. (2001).

### 3.2.2. Wolf-Rayet stellar component

The emission lines from the Wolf-Rayet component of the spectrum are summarized in Table 6. We used the complete line list for HII regions from García-Rojas et al. (2006), to separate out the HII lines. The optical spectrum we obtained shows strong emission in HeII 4686 and in NIII and NIV. These are characteristic of WN stars (see e.g. Niemela et al. 2006).

The X-ray emission with  $f_X = 2.6 \times 10^{-15} \text{ mW m}^{-2}$  has a soft spectrum ( $HR1 = -0.97$ ), which would be consistent with a SNR. However, the optical spectrum clearly indicates an HII region. There are wind-blown bubbles around O, B or WR stars, which are related to HII regions in that they are also regions of ionized gas surrounding a massive star (see Magnier et al. 1995). Wind-blown bubbles, from those around massive O and Wolf-Rayet stars to superbubbles around OB associations and Galactic winds in starburst galaxies, are X-ray emitters as most of their volume is taken up with hot gas,  $10^5 \leq T(K) \leq 10^8$ . Strickland & Stevens (1998) predict X-ray emission from wind-blown bubbles, which is soft but with possibly a hard tail.

Wolf-Rayet stars that are bright in X-rays are nearly always members of binary systems (Guerrero & Chu 2005). Many Wolf Rayet stars are binary systems. These often occur as W + O systems. As the O star plows through the thick wind from the WR star, a shock wave can be formed, often emitting X-rays. The X-ray survey of WR stars in the MCs has shown that WR stars in binary systems are much more frequently detected in X rays than single WR stars and that they have higher  $L_X/L_{bol}$  than apparently single WR stars. The X-ray luminosities of these X-ray-bright WR binaries are most likely enhanced by the colliding stellar winds: In a WR+OB binary system, the WR wind collides with the companion’s fast wind and generates shock-heated plasma at the interaction region. The X-ray luminosities of the WR stars in binaries the MCs span a wide range, from a few  $\times 10^{32}$  erg  $s^{-1}$  to  $\simeq 2 \times 10^{35}$  erg  $s^{-1}$  (Guerrero & Chu 2005).

Source M31\_146 is just above the detection limit of the X-ray survey ( $10^{35}$  erg  $s^{-1}$ ). It also has a soft spectrum. The combined X-ray and optical properties of the source are compatible with a WN and an O star binary, surrounded by an ionized bubble.

### 3.3. [PFH2005] 224 – M31 Supernova Remnant

Pietsch et al. (2005) classify this object as a supersoft source (although Stiele et al. 2011 do not). There are five candidate optical counterparts in LGGs (Massey et al. (2006)), four of which are very faint. On the  $H\alpha$  image there is clear indication of an SNR (ringlike  $H\alpha$  structure of 6 arcsec radius, with bright central spot). However, there is no previously published SNR (Blair et al. 1981; Magnier et al. 1995; Sasaki et al. 2012) at this location. On the other hand, Azimlu et al. (2011) record 3 HII regions within the error circle (IDs 1546, 1549, 1547).

We obtained spectra of both the brightest central candidate counterpart (LGGs\_J004210.24+405149.4) and of the faint adjacent object (LGGs\_J004210.38+405148.1). The optical spectrum of LGGs\_J004210.24+405149.4 referred to as object 224a, (Figures 7 and 8) has the characteristic emission lines with the expected line ratios (see description of object [PFH2005]146) for a SNR at the characteristic blueshift of M31,  $[SII]/H\alpha = 1.1$  and  $[OIII]/H\alpha = 0.7$ . We note that there are also weak Balmer lines and strong HeI lines in absorption, corresponding to an early type OB star. Therefore, there is light from an OB star contaminating the SNR spectrum. However, the line ratios and the soft X-ray characteristics confirms that the X-ray-emitting object is an SNR. It must be noted that a revised reduction of the XMM-Newton data (Stiele et al. 2011) yielded hardness ratios pointing to a harder source, although the errors are large. In an attempt to clarify the issue, we have searched in the *Chandra* archive for possible further information on this source. The source is visible on an ACIS-S (CCD no.6) 54ks exposure, as a faint soft source, with most of the photons below 1keV. The specific observation is far off axis, so it is not possible to determine if the source is a point source or extended. Therefore the *Chandra* observations seem to confirm that the source is soft rather than hard.

The spectrum of the second object, referred to as object 224b (LGGs\_J004210.38+405148.1,

Figure 9) shows only SNR emission lines at the blueshift of M31, with no visible stellar continuum.

In conclusion, the X-ray emission seems to be related to a newly identified SNR or superbubble, which is also positionally coincident with an OB star in M31. Single OB stars have been detected in X-rays and almost always show soft emission at characteristic temperatures  $kT < 1$  keV and low X-ray luminosities (Berghoefer et al. 1997), well below the detection limits of the *XMM-Newton* survey.

### 3.4. [Stiele2011] 235 – Strong M31 HMXB Candidate

There are two LGS objects within the error circle of the X-ray position, LGS\_J003937.29+404925.8 and LGS\_J003937.27+404928.9, both blue in colour. We have obtained spectra of both objects.

#### 3.4.1. LGS\_J003937.29+404925.8 – Emission line star

The blue and red spectra of LGS\_J003937.29+404925.8, the brightest and bluest of the two candidate counterparts, are shown in Figures 10 and 11, respectively. The spectra are blue-shifted by about  $-250 \text{ km s}^{-1}$ , indicating M31 membership. The blue part of the spectrum shows a relatively featureless continuum with very weak Balmer absorption and HeI absorption at  $4387\text{\AA}$ , almost as deep as  $H\gamma$ . Cross-correlation against our spectral standards found no correlation with our templates, likely due to the low S/N of the features. We have marked on the spectrum the location of the Balmer, HeI and HeII lines expected in early type (OB) stars. However, the S/N ratio is insufficient to identify with certainty any other absorption lines. There is also relatively strong emission at  $4508\text{\AA}$ , which is consistent with NIII ( $4511\text{-}4515\text{\AA}$ ), often seen in O stars. The weakness of the Balmer lines, the presence of some HeI in absorption and NIII in emission suggest a late O star. Using LGS photometric data we derive a value of  $\simeq -0.92$  for the reddening free Q-parameter, which is also consistent with an O9-B0 star, in agreement with our qualitative spectral classification. The derived Q-value is also well within the known range of Q values for Be stars (in the Galaxy the Q values of Be stars range between  $-0.322$  and  $-1.024$ ).

The red part of the spectrum shows clear  $H\alpha$  emission, with a FWHM of  $\simeq 7.7\text{\AA}$ , or  $\simeq 5.7\text{\AA}$  (corresponding to  $\simeq 240 \text{ km s}^{-1}$ ), after correcting for the spectral resolution. This value is quite normal for BeXRBs (e.g. BeXRBs in SMC cluster NGC330 Martayan et al. 2007).  $6560\text{\AA}$ ) Taking all the evidence into account, the star is of a late O-early B spectral type with apparently associated  $H\alpha$  emission.

In X-rays, the source is classified as a hard source, and its flux corresponds to an X-ray luminosity of  $L_X = 4.7 \times 10^{37} \text{ erg s}^{-1}$ . Most BeXRBs have X-ray luminosities  $\leq 3 \times 10^{36} \text{ erg s}^{-1}$ , but a few have been recorded up to  $10^{38} \text{ erg s}^{-1}$ .

The combination of optical and X-ray data make this object (LGS\_J003937.29+404925.8) a

very good HMXB candidate in M31, possibly a BeXRB.

There is however some evidence that reduces somewhat the confidence level of this classification. The  $H\alpha$  emission observed may be partly due to diffuse emission (from an HII region, not an SNR, because there is no [SII] visible in the spectrum): There is some indication of very weak diffuse  $H\alpha$  emission in the LGGS images around the position of LGGS\_J003937.29+404925.8. Moreover the spectrum shows some weak [NII] 6548Å emission which is consistent with nebular emission. Additionally, the second candidate counterpart discussed below also shows similar emission in  $H\alpha$ . Therefore, at least part of the  $H\alpha$  emission recorded maybe due to a small surrounding nebula.

### 3.4.2. *LGGS\_J003937.27+404928.9 – Early-type Star*

We have also obtained spectra for the fainter candidate optical counterpart LGGS\_J003937.27+404928.9. The blue spectrum is dominated by noise, with no spectral features identifiable. The red spectrum (12) shows  $H\alpha$  emission, with similar FWHM as in the case of LGGS\_J003937.29+404925.8. Using LGGS photometric data we derive a value of  $Q \simeq -0.83$  for the reddening free Q-parameter, which is consistent with a B0 star. Although the S/N of the spectra did not allow the spectral classification of LGGS\_J003937.27+404928.9, we cannot rule out the possibility that this star is the counterpart of the X-ray source. In this case as well, the object would be a good HMXB candidate.

## 3.5. [PFH2005] 242 – Foreground Star

This source has a soft X-ray spectrum in Stiele et al. (2011), making it unlikely to be an HMXB, but its bright blue counterpart candidate put it into our sample. There are four objects recorded in the Massey catalogue within the error circle of the revised X-ray position (Stiele et al. 2011), which will be discussed separately below.

### 3.5.1. *LGGS\_J004216.78+404814.4 – Chance Superposition*

This is one of the two brighter objects in the error circle, for which we have obtained an optical spectrum. The magnitude and colours ( $V = 19.419 \pm 0.004$   $B - V = -0.104 \pm 0.005$ ,  $U - B = -0.993 \pm 0.004$ ,  $V - R = -0.013 \pm 0.006$   $R - I = -0.010 \pm 0.005$ ) are consistent with an OB dwarf in M31. The spectrum obtained (Figure 13) is almost entirely featureless, indicative of an OB dwarf at this luminosity. The  $H\alpha$  line appears in absorption at 6554Å, blue-shifted by about  $410 \text{ km s}^{-1}$ . There is a weak HeI 6678 line appearing at 6669Å at the same blueshift as  $H\alpha$ , which confirms its identification. There is also a marginal detection of HeII ( $\lambda 4541$ ) line at the same blueshift (observed at  $\simeq 4535\text{Å}$ ). These line identifications confirm that the star is of O9-BO spectral type. The spectral type is also consistent with the value of the reddening free Q

parameter ( $Q_{UBV} = -0.918 \pm 0.006$ ). The star is also on the locus of Be stars on the U-B vs B-V diagram (Feinstein & Marraco 1979). However, the hardness ratios obtained for the X-ray source are inconsistent with the BeXRB. Actually, they are more consistent with a foreground star (*cf.* Table 2).

In conclusion, the observed brightest optical counterpart of [PFH 2005] 242 is an early type OB star in M31, with no H $\alpha$  emission. The inconsistency of the X-ray hardness ratios with a HMXB render the probability that this is the correct counterpart of the X-ray source low. Therefore we consider the rest of the optical sources in the X-ray error circle, in the following subsections.

### 3.5.2. *LGGS J004216.61+404815.9 – Chance Superposition*

This object is much fainter, very red and probably extended.  $V = 22.602 \pm 0.061$   $B - V = 1.817 \pm 0.477$ ,  $V - R = 0.895 \pm 0.071$ ,  $R - I = 0.911 \pm 0.037$ . Assuming that the object is in M31 ( $m - M_0 = 24.47$ , and  $E(B - V) = 0.08$  McConnachie et al. 2005), we would have  $M_V \simeq -1.9$ ,  $(B - V)_o \simeq 1.74$ ,  $(V - I)_o \simeq 1.7$ , which are not consistent with any stellar object in M31.

### 3.5.3. *LGGS\_J004216.47+404812.0 – Foreground Star*

This object is red ( $V = 19.843 \pm 0.004$ ,  $B - V = 1.575 \pm 0.011$   $U - B = 1.126 \pm 0.024$   $V - R = 1.007 \pm 0.005$   $R - I = 1.114 \pm 0.004$ ), with colours consistent with late K -early M star. This may be a Galactic foreground object with proper motion  $\text{pm}_{\text{RA}} = -41.5 \pm 5.7 \text{ mas yr}^{-1}$   $\text{pm}_{\text{DEC}} = -41.3 \pm 5.7 \text{ mas yr}^{-1}$  (Roeser et al. 2010) and IR photometry from 2MASS 00421645+4048113 J=16.381(0.117). This foreground star could be the counterpart of the X-ray source.

### 3.5.4. *LGGS\_J004216.52+404810.2 – Foreground Star*

This object is also red ( $V = 22.013 \pm 0.020$ ,  $B - V = 1.531 \pm 0.125$ ,  $U - B = 99.999 \pm 99.999$ ,  $V - R = 0.875 \pm 0.024$ ,  $R - I = 1.030 \pm 0.013$ ). The colours are consistent with a Galactic M-dwarf, also making this star a possible counterpart candidate.

Therefore, most probably this X-ray source can be identified with a foreground M star.

## 3.6. [PFH2005] 246 – M31 Globular Cluster LMXB

According to a recent catalogue of globular cluster GCs in M31 (Caldwell et al. 2009), at the position of the X-ray source, there is an old GC named B086-G148 (0:42:18.65, 41:14:02.1). The X-ray source has been widely discussed in the literature (Trinchieri & Fabbiano 1991; Primini et al.

1993; Supper et al. 1997; Voss & Gilfanov 2007, e.g.). The optical spectrum (Figure 14) is consistent with that of a GC, with characteristic Balmer lines, H and K CaII and G-band, as expected from the composite spectrum of a GC (e.g., Galleti et al. 2007). Therefore, this is most likely an LMXB in the GC.

### 3.7. [PFH2005] 278 – Strong M31 HMXB Candidate

The optical counterpart candidate observed is LGGJ004231.23+410435.3. It is the brightest star in the LGGJ catalogue lying within the 3-sigma error circle of the X-ray position. There is one other faint object (LGGJ004231.38+410436.1) within the error circle which will be discussed as well. The optical spectrum of LGGJ004231.23+410435.3 (Figure 15) has relatively low S/N, resulting in no conclusive cross-correlation results, but some lines can be identified at low significance; the strongest feature is  $H\beta$  at the blueshift of M31 at  $\simeq -400 \text{ km s}^{-1}$ . At about the same blueshift there are some HeI and weak HeII absorption lines, as well as OII in absorption, and probable emission in SiIV and NIII. Despite the low S/N the consistency of the blueshifts of the tentative lines increase confidence in their identification. The red part of the spectrum is of low S/N because the star is blue, and detects no features. Nonetheless, because the  $H\alpha$  line is not seen either in emission or in absorption, it may be filled-in by emission.

The identified lines are characteristic of an early type star around B0, while the observed emission lines are most probably indicative of a supergiant, although they are not typical. The magnitude and colours of the star given in LGGJ are consistent with a B0-B0.5 II-Ib supergiant, in agreement with the spectral classification. Thus this is a high-mass star in M31 with some interesting emission. Furthermore, it is reported as a variable source in the POINT-AGAPE survey (Period= $10^3.080$  days (with a false alarm probability of  $10^{-32.9}$ ), An et al. 2004). The X-ray flux of the source at the distance of M31 is  $\simeq 1.7 \times 10^{36} \text{ erg s}^{-1}$ , while it is classified as a hard source in both PFH2005 and Stiele et al. (2011). All of these characteristics make [PFH2005] 278 a good HMXB candidate, probably a SG-XRB.

It must be noted that there is another much fainter object ( $V = 22.07$ ) recorded in LGGJ (LGGJ004231.38+410436.1) within the error circle. The object is rather red ( $B-V = 1.43 \pm 0.21$ ), consistent with a K-M type star, probably a foreground dwarf. The X-ray properties of the X-ray source are not consistent with a <fg> classification; therefore, this fainter object is not a probable counterpart for the X-ray source.

### 3.8. [PFH2005] 367 – M31 HMXB Candidate

Within the [PFH2005] 3-sigma error circle of the source there are three sources recorded in the Massey et al. (2006) catalogue, namely objects LGGJ004258.94+413727.3, LGGJ004259.07+413731.4 and LGGJ004259.02+413730.9. We obtained spectra for the first and second object, as the third

one is too faint ( $V = 21.55$ ).

### 3.8.1. *LGGS\_J004258.94+413727.3 – OB Supergiant*

This is the brightest and bluest of the objects within the 3-sigma error circle of the X-ray source.

The spectrum obtained is contaminated somewhat by LGGS\_J004258.99+413726.8 (just outside the error circle,  $0.75''$  from LGGS\_J004258.94+413727.3), which is however 1 mag fainter (but also blue), therefore the prevailing spectrum is that of LGGS\_J004258.94+413727.3. The spectrum is shown in Figure 16. The Balmer lines appear in absorption, at a velocity of  $\simeq -320$  km s $^{-1}$ , compatible with M31 membership. The spectrum cross-correlates with VOR+59 97 (B2 V) at a velocity of  $-390 \pm 110$  km s $^{-1}$ , and with HD 13799 (B6 III) at a velocity of  $-350 \pm 60$  km s $^{-1}$ . There are clear He I lines as well as MgII (4481Å) and SiIII (4128Å). Using the criteria of Evans et al. (2004) the star appears to be a late B star, probably B9. However, the strength of the SiIII (4553Å) line in comparison to the MgII4481 line is pointing to an earlier type, around B3. There is also weak emission of NIII (4373Å) which is seen in O stars. However, there are no HeII lines anywhere in the spectrum, as would be expected for an O star. In the red part of the spectrum the only clearly identifiable line is H $\alpha$  in absorption. The reddening free Q-parameter of the star on the basis of the LGGS colours is  $Q = -1.19$ , which is not compatible with a late B star, but rather with an O star. The magnitude of the star at the distance of M31 (and accounting for the average interstellar absorption) corresponds to  $M_V \simeq -4.8$  which is marginally consistent with a relatively late O star or a late B Iab supergiant (cf Wegner 2006). As there are indications that the spectrum is a composite spectrum of two early type stars, it is possible that the LGGS magnitude is not of a single star, therefore the magnitude may be overestimated. However, the most probable interpretation of the data is that of an OB supergiant of the Iab type, showing no H $\alpha$  emission. The X-ray characteristics of the source are consistent with a HMXB, with an X-ray flux of  $\simeq 8 - 9 \times 10^{35}$  erg s $^{-1}$ .

This object is recorded by Vilardell et al. (2006) as a low amplitude variable in M31, M31V\_J00425892+4137271 (V=19.546, B=20.742), with a period of 87.78days, but with no further classification.

### 3.8.2. *LGGS\_J004259.07+413731.4 – Chance Superposition*

This object has the spectrum of an M5 foreground star (see Figure 17), and shows no significant variability (Vilardell et al. 2006). It must be noted that the colours recorded in LGGS for this star are not consistent with the spectral type of the star, and would correspond to an earlier spectral type. The spectral classification however overwrites the photometric information from LGGS. While such stars can be X-ray-producing systems, (e.g. in symbiotic X-ray binaries Corbet et al. 2008), they would be expected to have a much softer X-ray spectrum than observed.

In conclusion, the early type Iab supergiant LGGJ004258.94+413727.3 is the most probable optical counterpart of the X-ray source, and therefore the object is a probable HMXB (SG-XRB).

### 3.9. [PFH2005] 405 – M31 LMXB in a Star Cluster

There is one optical counterpart in the LGGJ catalogue within the 3-sigma error circle of the X-ray source position, LGGJ004309.86+411900.9. There is a confirmed (unresolved) globular cluster, SK059A (10.791125, 41.31700) registered at this position in the Revised Bologna catalogue of M31 globular clusters, first recorded in the survey of Kim et al. (2007). However, the *optical* flux of the object is known to be variable (R-band period of  $434 \pm 4$  days and I-band period of  $385 \pm 16$  d; Fliri et al. 2006). Fliri et al. classify it as a semi-regular red variable.

The source correlates also with an unresolved radio source 37W153 (S1412MHz= $1.1 \pm 0.2$  mJy Walterbos et al. 1985). Finally, the object has also been classified as an HII region by Caldwell et al. (2009) and Peacock et al. (2010).

In X-rays, the source is transient (Williams et al. 2004, 2006). Its variability has been studied by Hofmann et al. (2013), who classify the X-ray lightcurve as highly variable.

The optical spectrum we have obtained is consistent with a relatively late type star, and resembles a K supergiant (K2Iab), with significant H $\alpha$  absorption (as expected for early K supergiants, see e.g. Mallik 1986). The spectrum (see Figure 18) is very similar for example to that of the K3Iab supergiant BN Car. The spectrum allows the possibility of a globular cluster, but is inconsistent with this hypothesis in two ways: there is H $\alpha$  absorption, and there is indication of emission lines in [OIII] (5007Å) and [NII] (6584Å). The spectrum is blue-shifted by  $\simeq 180$  km s $^{-1}$  consistent with M31 membership.

The LGGJ colours are entirely consistent (comparison with standard values from Allen’s Astrophysical quantities 4th edition) with an early K giant and marginally consistent with a K0 (or late G) supergiant, while the absolute magnitude at  $M_V \simeq -6.3$  is only consistent with an early K or late G supergiant. The infrared colours available from 2MASS are compatible with a K5Iab supergiant (or a bit later type).

The long period optical variability, radio emission, optical spectrum and optical and infrared colours therefore strongly suggest that this is a red long-period variable supergiant star.

The X ray source is highly variable and relatively hard (not as hard as BeXRBs). If it is connected to the globular cluster then it is a LMXB. If it is connected with the massive red supergiant, then it would be an accreting binary, as single late type supergiants can emit X-rays (e.g. FK Comae stars) only at much lower luminosities ( $\gtrsim 10^{32}$  erg s $^{-1}$ ). Given the late spectral type, the object cannot be a HMXB (as the massive star in these cases has spectral type O or B). So the object may belong to the poorly populated class of symbiotic X-ray binaries, like XTE J1743-363 (Smith et al. 2012). These types of objects can have X-ray luminosities from few  $10^{32}$

to  $10^{37}$  erg s $^{-1}$  (Postnov et al. 2010).

As the presence of a globular cluster is rather certain, with the source being definitely extended (and not an HII region as no characteristic lines were seen), it is also possible that there is a bright long period variable coinciding in location with the cluster. In this case the source is most probably connected with the GC, and it is a LMXB. If the radio emission is also connected to the same source it could point to a microquasar.

### 3.10. [PFH2005] 407 – Strong M31 BeXRB Candidate

There are two counterparts in the LGGs catalogue within the 3-sigma error circle of the X-ray source, LGGs\_J004310.5+413852.0 and LGGs\_J004310.43+413854.7. We obtained a spectrum of the former, which is the brightest of the two, at  $V=19.96$  mag. The second candidate counterpart is a faint blue object with  $V = 21.39$

The spectrum of LGGs\_J004310.5+413852.0 is shown in Figure 19 and in Figure 20. It shows characteristic Balmer and HeI absorption lines at a velocity of  $-100$  km s $^{-1}$ . Cross-correlation is good with VOR+59 97 (B2 V) and a velocity of  $-140\pm 100$  km s $^{-1}$ , in agreement with our qualitative assessment.

The HeI lines clearly classify the star as a B star. The magnitude, colours and reddening free Q-parameter from LGGs (see Table 3) are entirely consistent with an early B star in M31. In the red part of the spectrum, there is significant H $\alpha$  emission, with a FWHM of  $7.2\text{\AA}$  (after correcting for the spectral resolution, as for source 235 above). The star is a known emission-line star (Massey et al. 2007) with H $\alpha$  magnitude of 19.72. Due to its proximity to an HII region (also recorded as a SNR candidate 89A; Braun & Walterbos 1993) just outside the error circle (HII region ID2013; Azimlu et al. 2011), the spectrum may be contaminated by diffuse emission, however, the H $\alpha$  image of the area shows no diffuse emission at the location of the star. Therefore the H $\alpha$  emission seems to be related to the B star (but some contamination is also possibly present). Interestingly, the star is reported as showing significant variability in the optical, with a period of 15.802446d (Vilardell et al. 2006). In X-rays the source is classified as hard and the hardness ratios are consistent with BeXRBs (see discussion). The X-ray luminosity of the source is  $\simeq 3.6 \times 10^{35}$  erg s $^{-1}$ .

Therefore, the Be stellar counterpart and X-ray properties are entirely consistent with a BeXRB. This is the first BeXRB identified with some certainty in M31.

### 3.11. [PFH2005] 466 – M31 Supergiant HMXB candidate

There are two possible counterparts in the LGGs catalogue within the X-ray position error circle. The brightest and bluest, LGGs\_J004333.64+411404.8, was the one observed. The other

object, LGGJ004333.59+411407.7, is two magnitudes fainter and redder.

The spectrum is blue-shifted by about  $-200 \text{ km s}^{-1}$ , confirming M31 membership. The spectrum shows a correlation peak with VOR+59 97 (B2 V) with a velocity of  $-130 \pm 80 \text{ km s}^{-1}$ . The blue part of the spectrum of LGGJ004333.64+411404.8 (Figure 21) shows HeI (4009 and 4471) and possibly SiIII 4028-30 absorption lines consistent with a B star. The red part of the spectrum (Figure 22) shows strong NIII $\lambda$ 6610 emission, normally seen in later type O supergiants (Walborn 2001). For such a spectral type one would also expect HeII lines, which are probably too weak for the S/N ratio of our spectra. Certainly the presence of HeI rules out any spectral type earlier than O9. According to the Atlas of Walborn & Fitzpatrick (1990), the spectral characteristics of LGGJ004333.64+411404.8 may also be consistent with ON9.7Ia+.

The optical magnitude and colours, as well as the value of the reddening free Q-parameter of LGGJ004333.64+411404.8 (see Table 3) are more consistent with a relatively heavily reddened B-type supergiant. The Q-parameter value of  $-0.69$  points toward an early B star, between B1 and B3 depending on the luminosity class. Given the V magnitude of 19.49 and estimating the reddening from the observed  $B - V = 0.544$  and the estimated  $B - V \simeq -0.2$  to  $-0.1$ , according to the Q-parameter value, we estimate an absolute magnitude around  $-6.5$  consistent with an O9 supergiant. In conclusion, we classify the object as an OB supergiant.

Young O stars are strong, hard, and variable X-ray sources that often dominate the X-ray emission from young clusters, but their X-ray luminosities only extend up to  $L_X = 10^{34} \text{ erg s}^{-1}$ . Therefore, because of the high X-ray luminosity ( $\sim 5 \times 10^{35} \text{ erg s}^{-1}$  of [PFH2005] 466, the observed X-rays are more likely from accretion onto a compact companion to this O-supergiant, making this source a good HMXB candidate, of the SgXRB type.

### 3.12. [PFH2005] 581 – Galactic CV

There are two counterparts in the Massey catalogue, the brightest and bluest is LGGJ004445.06+415153.4, which we observed, and a fainter also quite blue object LGGJ004444.97+415151.3.

The optical spectrum of LGGJ004445.06+415153.4 (Figure 23) shows significant emission lines of CII (4267, 4738, 4745Å), as well as H-beta in emission (H-gamma seems to be filled-in by emission; earlier Balmer lines seen in absorption) and weak CIII emission (4187Å). There is also clear absorption of HeI4026. Such a spectrum is reminiscent of a cataclysmic variable (dwarf nova) in eruption (e.g., Joergens et al. 2000), although it lacks the expected HeI and HeII emission lines that should also be present in such spectra. The blue colour, characteristic emission lines, X-ray emission and relatively low velocity ( $\simeq 50 \text{ km s}^{-1}$ , are consistent with a foreground cataclysmic variable. As the X-ray spectrum is hard, the object is most probably an intermediate polar with expected  $L_X \simeq 10^{31} - 10^{33} \text{ erg s}^{-1}$  (which is also consistent with the observed X-ray flux of  $1.8 \times 10^{-14} \text{ mW m}^{-2}$ , since the source is within the Galaxy).

### 3.13. [PFH2005] 599 – Chance Superposition

There is only one optical counterpart candidate listed in LGGs, LGGs\_J004456.78+413548.0. The spectrum of this faint blue counterpart candidate (Figure 24) shows weak Balmer and HeI absorption lines, characteristic of an early B star, and no emission lines. Its radial velocity is redshifted by  $\simeq 80 \text{ km s}^{-1}$ , showing that it is a foreground object. The X-ray source is hard and weak. The optical spectrum is not consistent with a cataclysmic variable. Therefore, most probably the object observed is not the correct counterpart. Within the X-ray position error circle ( $3\sigma$ ;  $5.26''$ ) there are several faint sources visible in the LGGs images, although they are not catalogued. Vilardell et al. (2006) list 7 faint sources in addition to LGGs\_J004456.78+413548.0, within the error circle. They range in magnitude between  $V = 21.8$  and  $V = 24.8$  mag. The brightest of the seven is a blue variable star, M31V\_J00445707+4135466, with a period of 80d. Further observations are needed to identify the optical counterpart of the X-ray source [PFH2005]599.

### 3.14. [PFH2005] 612 – M31 HMXB candidate

There is a single source catalogued in LGGs within the 3-sigma error circle of the X-ray source, object LGGs\_J004506.46+420615.8. The spectrum obtained for the star suffers from relatively low S/N (Figure 25), however, it does show a strong blue continuum with Balmer and HeII lines as well as possible CII in absorption, blueshifted by about  $-150 \text{ km s}^{-1}$ , which is consistent with M31 membership. The spectrum is consistent with a mid-to late O dwarf star in M31. Cross-correlation peaks with B+57 18 (B3 IV) with a velocity of  $-110 \pm 160 \text{ km s}^{-1}$ , so reddening may be affecting the correlation, but in any case, it is an early-type star in M31.

In the red part of the spectrum  $H\alpha$  is not resolved. It is either filled in by emission and/or weak and blended with adjacent HeII lines ( $6527\text{\AA}$ ,  $6560\text{\AA}$ ).

The optical magnitude and colours, as well as the value of the reddening free Q-parameter of LGGs\_J004506.46+420615.8 (see Table 3) are also consistent with a O5-O9 main sequence star in M31.

The X-ray properties of the source indicate a hard spectrum and a luminosity of  $L_X = 5.2 \times 10^{35} \text{ erg s}^{-1}$ .

The early spectral type (late O) of the star and its X-ray properties are consistent with a HMXB, however the lack of significant  $H\alpha$  emission weakens the identification of the source with a BeXRB. It must also be noted that although the star appears to be a single counterpart in the LGGs catalogue, inspection of the images shows other possible fainter counterparts within the error circle, some of which are particularly visible in the  $I$  image.

Overall, the source is an HMXB candidate, but not one of our strongest.

### 3.15. [PFH2005] 620 – M31 HMXB Candidate

Within the error circle of the X-ray position (3sigma 4.26") there is one object recorded in LGGs, LGGs\_J004513.59+413805.7, although in the near infrared image at least another five very faint sources are visible. Indeed, Vilardell et al. (2006) report another 8 faint objects within the 3sigma error circle of the X-ray source position with V magnitudes between 22.35 and 24.77 mag. The spectrum of the single LGGs counterpart is shown in Figure 26. The star has a blue continuum with Balmer lines in absorption, no later than late B (from the appearance of the Balmer lines). The S/N does not allow accurate classification of the spectrum, however there are indications of some HeI and CII absorption lines. No emission lines are seen in the spectrum. The H $\alpha$  line is also seen in absorption. The velocity of the star ( $\simeq -200$  km s $^{-1}$ ) is consistent with M31 membership. Cross-correlation yields plausible peaks with several of our B-type standards, including VOR+59 97 (B2 V) with a velocity of  $-160 \pm 110$  km s $^{-1}$ . The magnitude and colours given in LGGs for the observed star (see Table 3) do not provide a consistent classification for the object: the reddening free Q parameter value around 0 suggests a late B or early A star, while the V magnitude is too bright for such a late type star (unless it is a supergiant). It is possible that the photometry is contaminated by nearby faint objects. The X-ray properties of the source suggest a hard spectrum and a luminosity of  $5.7 \times 10^{35}$  erg s $^{-1}$ .

Thus, this is still a HMXB candidate, but not one of the better candidates due to the lack of emission lines, and relatively uncertain spectral classification.

### 3.16. [PFH2005] 705 – Chance Superposition

There is a single counterpart in the LGGs catalogue for this object, LGGs\_J004604.83+415142.4. The spectrum shows a F-G foreground star with no H $\alpha$  emission. The X-ray source is classified as hard, on the basis of its hardness ratio values, therefore the star observed is not the correct counterpart. On the LGGs images there are more than three faint red objects within the 3-sigma error circle, which are candidate counterparts, which however are not recorded in Massey et al. (2006).

### 3.17. [Stiele2011] 1716 – M31 HMXB Candidate

There is a single counterpart candidate in the LGGs catalogue within the X-ray error circle, LGGs\_J004557.04+414830.0, with  $V = 20.017$  and  $B - V = 0.123$ . Except for this relatively bright blue object, there appears to be another object within the error circle, visible in the near infrared image, but not recorded in the LGGs catalogue. This very red object is also recorded in 2MASS (2MASS J00455703+4148322) and in the WISE All-Sky data release catalogue (WISE J004556.96+414832.3, Cutri & et al. 2012).

We have obtained a spectrum for the bright blue counterpart LGGJ004557.04+414830.0. The blue part of the spectrum (see Figure 27) reveals a hot star with Balmer line absorption, and two CII line pairs that can be identified with relative certainty, CII4738+4745, CII4289+4293.7, which are common features in the spectra of Be stars. The Balmer lines from H $\epsilon$  to H $\beta$  are clearly seen in absorption at a velocity of  $\simeq$ -260 km s $^{-1}$ , confirming M31 membership. Cross-correlation yields peaks with VOR+59 97 (B2 V) at a velocity of  $-170\pm 160$ . The red part of the spectrum (see Figure 28) shows the H $\alpha$  line almost completely filled in with emission, resulting in a very weak line. This is a known feature of Be stars. To classify the star as a Be star, the H $\alpha$  line should be seen in emission. In this case, the line is almost completely filled in, which indirectly indicates emission. Therefore, the object is likely a Be star. The hardness ratios are completely consistent with the SMC BeXRBs. The X-ray flux corresponds to  $5.1 \times 10^{36}$  erg s $^{-1}$ . Therefore, the object is a good candidate BeXRB in M31.

#### 4. Discussion and Conclusions

Table 7 summarizes our classifications, on the basis of the spectral characteristics of the candidate optical counterparts. In all but two cases we have identified a source that could provide the observed X-ray emission. Among these objects, there are 8 that are possible (5) or probable (3) high mass XRB in M31. We provide their radial velocities, along with the velocity of the M31 gas disc at their projected location (as determined from the 21 cm maps of Chemin et al. 2009) in Table 8. The velocities are in general agreement with ours, which have relatively low  $\sim$ 100 km s $^{-1}$  precision. The largest outlier is [PMH 235], which is 200 km s $^{-1}$  different from the local gas, but still not enough different to suggest that it is a high velocity star.

It is interesting to examine the location of these objects in characteristic diagrams in the optical and in the X-rays, in comparison to the loci of confirmed HMXBs of other galaxies on the same diagrams. Figure 29 shows a diagram of apparent magnitude versus the reddening free Q-parameter  $Q = U - B - 0.72(B - V)$ , for all stars in the LGGJ-M31 catalogue with both U-B and B-V colours measured (grey dots). The Q parameter is used instead of the customary B-V colour, in order to compensate for the variable reddening to the individual sources of interest here. Clearly, all but one of the HMXB candidates lie within the expected locus. Object 620 lies outside the box, however the spectral class is consistent with an early type star, suggesting a problem with the LGGJ colours for this star.

Figure 30 shows a X-ray hardness ratio diagram, of HR4 versus HR3 (see Table 2). With blue dots we mark the location of confirmed BeXRBs in the Small Magellanic Cloud (SMC), while with red dots of confirmed AGNs behind the SMC, from (Sturm et al. 2013). In grey we show the location of class A and class B HMXB candidates from Table 7. Generally, BeXRBs and AGNs are relatively well separated on this diagram in the SMC, although there is overlap. Our candidates lie within the locus of the SMC BeXRBs, taking into account the observational errors, although on average they are somewhat softer than the SMC objects. Indeed, our only BeXRB candidate

(407) lies within the SMC locus, and so does 1716st which is classified as a probable HMXB, but as mentioned above the absence of  $H\alpha$  absorption probably indicates emission that fills in the absorption line, which would make the object a very good BeXRB candidate.

In conclusion, we have observed, reduced, and classified 20 spectra of bright blue optical counterpart candidates of 17 X-ray sources in the M31 field. We have found 3 strong HMXB candidates, and 5 acceptable candidates in the field of M31. These are likely only a fraction of the HMXBs in M31 when compared to expectations based on the star formation rate and comparisons with the Galaxy. Significantly more could be found with improved data sets. For example, precise source locations could be obtained by *Chandra* imaging and matched with deeper and better-resolved stellar photometry, such as that of the Panchromatic Hubble Andromeda Treasury (Dalcanton et al. 2012, Williams et al., in prep.).

While our candidates require very high-quality spectral follow-up on larger telescopes in order to look for radial velocity variations that would confirm their HMXB nature, the relative numbers, optical spectra, optical photometry, and X-ray properties of our best HMXB candidates suggests they should be the focus of dedicated high signal-to-noise studies at higher spectral resolution in the future.

Support for this work was provided by NASA under grant NNX06AF58G.

## REFERENCES

- An, J. H., et al. 2004, MNRAS, 351, 1071
- Azimlu, M., Marciniak, R., & Barmby, P. 2011, AJ, 142, 139
- Baade, W., & Arp, H. 1964, ApJ, 139, 1027
- Barnard, R., Garcia, M. R., & Murray, S. S. 2013, ApJ, 770, 148
- Berghoefer, T. W., Schmitt, J. H. M. M., Danner, R., & Cassinelli, J. P. 1997, A&A, 322, 167
- Blair, W. P., Kirshner, R. P., & Chevalier, R. A. 1981, ApJ, 247, 879
- Braun, R. 1990, ApJS, 72, 761
- Braun, R., & Walterbos, R. A. M. 1993, A&AS, 98, 327
- Caldwell, N., Harding, P., Morrison, H., Rose, J. A., Schiavon, R., & Kriessler, J. 2009, AJ, 137, 94
- Chemin, L., Carignan, C., & Foster, T. 2009, ApJ, 705, 1395
- Corbet, R. H. D., Sokoloski, J. L., Mukai, K., Markwardt, C. B., & Tueller, J. 2008, ApJ, 675, 1424

- Cutri, R. M., & et al. 2012, *VizieR Online Data Catalog*, 2311, 0
- Dalcanton, J. J., et al. 2012, *ApJS*, 200, 18
- Downes, R. A., Webbink, R. F., Shara, M. M., Ritter, H., Kolb, U., & Duerbeck, H. W. 2001, *PASP*, 113, 764
- Dray, L. M. 2006, *MNRAS*, 370, 2079
- Drissen, L., Crowther, P. A., Úbeda, L., & Martin, P. 2008, *MNRAS*, 389, 1033
- Evans, C. J., Howarth, I. D., Irwin, M. J., Burnley, A. W., & Harries, T. J. 2004, *MNRAS*, 353, 601
- Feinstein, A., & Marraco, H. G. 1979, *AJ*, 84, 1713
- Fliri, J., Riffeser, A., Seitz, S., & Bender, R. 2006, *A&A*, 445, 423
- Galleti, S., Bellazzini, M., Federici, L., Buzzoni, A., & Fusi Pecci, F. 2007, *A&A*, 471, 127
- Garcia, M. R., et al. 2010, *ApJ*, 710, 755
- García-Rojas, J., Esteban, C., Peimbert, M., Costado, M. T., Rodríguez, M., Peimbert, A., & Ruiz, M. T. 2006, *MNRAS*, 368, 253
- Grimm, H.-J., Gilfanov, M., & Sunyaev, R. 2002, *A&A*, 391, 923
- Grimm, H.-J., Gilfanov, M., & Sunyaev, R. 2003, *MNRAS*, 339, 793
- Guerrero, M. A., & Chu, Y.-H. 2005, in *Massive Stars and High-Energy Emission in OB Associations*, ed. G. Rauw, Y. Nazé, R. Blomme, & E. Gosset, 13
- Hofmann, F., Pietsch, W., Henze, M., Haberl, F., Sturm, R., Della Valle, M., Hartmann, D. H., & Hatzidimitriou, D. 2013, *A&A*, 555, A65
- Holland, S., Fahlman, G. G., & Richer, H. B. 1996, *AJ*, 112, 1035
- Joergens, V., Mantel, K.-H., Barwig, H., Bärnbantner, O., & Fiedler, H. 2000, *A&A*, 354, 579
- Kaaret, P. 2002, *ApJ*, 578, 114
- Kewley, L. J., Heisler, C. A., Dopita, M. A., & Lumsden, S. 2001, *ApJS*, 132, 37
- Kim, S. C., et al. 2007, *AJ*, 134, 706
- Kraemer, K. E., Price, S. D., Mizuno, D. R., & Carey, S. J. 2002, *AJ*, 124, 2990
- Liu, Q. Z., van Paradijs, J., & van den Heuvel, E. P. J. 2000, *A&AS*, 147, 25
- Long, K. S., Charles, P. A., & Dubus, G. 2002, *ApJ*, 569, 204

- Magnier, E. A., Prins, S., van Paradijs, J., Lewin, W. H. G., Supper, R., Hasinger, G., Pietsch, W., & Truemper, J. 1995, *A&AS*, 114, 215
- Mallik, S. V. 1986, *MNRAS*, 222, 307
- Martayan, C., Floquet, M., Hubert, A. M., Gutiérrez-Soto, J., Fabregat, J., Neiner, C., & Mekkas, M. 2007, *A&A*, 472, 577
- Massey, P., McNeill, R. T., Olsen, K. A. G., Hodge, P. W., Blaha, C., Jacoby, G. H., Smith, R. C., & Strong, S. B. 2007, *AJ*, 134, 2474
- Massey, P., Olsen, K. A. G., Hodge, P. W., Strong, S. B., Jacoby, G. H., Schlingman, W., & Smith, R. C. 2006, *AJ*, 131, 2478
- Matonick, D. M., & Fesen, R. A. 1997, *ApJS*, 112, 49
- McConnachie, A. W., Irwin, M. J., Ferguson, A. M. N., Ibata, R. A., Lewis, G. F., & Tanvir, N. 2005, *MNRAS*, 356, 979
- Niemela, V. S., Gamen, R. C., Solivella, G. R., Benaglia, P., Reig, P., & Coe, M. J. 2006, in *Revista Mexicana de Astronomia y Astrofisica*, vol. 27, Vol. 26, *Revista Mexicana de Astronomia y Astrofisica Conference Series*, 39
- Orosz, J. A., et al. 2007, *Nature*, 449, 872
- Peacock, M. B., Maccarone, T. J., Knigge, C., Kundu, A., Waters, C. Z., Zepf, S. E., & Zurek, D. R. 2010, *MNRAS*, 402, 803
- Pellet, A., Astier, N., Viale, A., Courtes, G., Maucherat, A., Monnet, G., & Simien, F. 1978, *A&AS*, 31, 439
- Pietsch, W., Freyberg, M., & Haberl, F. 2005, *A&A*, 434, 483
- Pietsch, W., et al. 2009, *ApJ*, 694, 449
- Pietsch, W., Haberl, F., Sasaki, M., Gaetz, T. J., Plucinsky, P. P., Ghavamian, P., Long, K. S., & Pannuti, T. G. 2006, *ApJ*, 646, 420
- Postnov, K., et al. 2010, in *Eighth Integral Workshop. The Restless Gamma-ray Universe (INTEGRAL 2010)*
- Primini, F. A., Forman, W., & Jones, C. 1993, *ApJ*, 410, 615
- Roeser, S., Demleitner, M., & Schilbach, E. 2010, *AJ*, 139, 2440
- Rosino, L. 1973, *A&AS*, 9, 347
- Sabogal, B. E., Mennickent, R. E., Pietrzyński, G., & Gieren, W. 2005, *MNRAS*, 361, 1055

- Samus, N. N., Durlevich, O. V., & et al. 2009, *VizieR Online Data Catalog*, 1, 2025
- Sasaki, M., Pietsch, W., Haberl, F., Hatzidimitriou, D., Stiele, H., Williams, B., Kong, A., & Kolb, U. 2012, *A&A*, 544, A144
- Schiavon, R. P., Barbuy, B., Rossi, S. C. F., & Milone, A. 1997, *ApJ*, 479, 902
- Sharov, A. S., & Alksnis, A. K. 1989, *Soviet Astronomy Letters*, 15, 382
- Shtykovskiy, P., & Gilfanov, M. 2005, *MNRAS*, 362, 879
- Smith, D. M., Markwardt, C. B., Swank, J. H., & Negueruela, I. 2012, *MNRAS*, 422, 2661
- Stiele, H., Pietsch, W., Haberl, F., Hatzidimitriou, D., Barnard, R., Williams, B. F., Kong, A. K. H., & Kolb, U. 2011, *A&A*, 534, A55
- Strickland, D. K., & Stevens, I. R. 1998, *MNRAS*, 297, 747
- Sturm, R., et al. 2013, *A&A*, 558, A3
- Supper, R., Hasinger, G., Pietsch, W., Truemper, J., Jain, A., Magnier, E. A., Lewin, W. H. G., & van Paradijs, J. 1997, *A&A*, 317, 328
- Tovmasyan, G. G. 1984, *Astrophysics*, 21, 507
- Trinchieri, G., & Fabbiano, G. 1991, *ApJ*, 382, 82
- Vilardell, F., Ribas, I., & Jordi, C. 2006, *A&A*, 459, 321
- Voss, R., & Gilfanov, M. 2007, *MNRAS*, 380, 1685
- Walborn, N. 2001, in *Astronomical Society of the Pacific Conference Series*, Vol. 242, *Eta Carinae and Other Mysterious Stars: The Hidden Opportunities of Emission Spectroscopy*, ed. T. R. Gull, S. Johannson, & K. Davidson, 217
- Walborn, N. R., & Fitzpatrick, E. L. 1990, *PASP*, 102, 379
- Walterbos, R. A. M., Brinks, E., & Shane, W. W. 1985, *A&AS*, 61, 451
- Warner, B. 1995, *Cambridge Astrophysics Series*, 28
- Watson, C., Henden, A. A., & Price, A. 2013, *VizieR Online Data Catalog*, 1, 2027
- Williams, B. F. 2003, *AJ*, 126, 1312
- Williams, B. F., Garcia, M. R., Kong, A. K. H., Primini, F. A., King, A. R., Di Stefano, R., & Murray, S. S. 2004, *ApJ*, 609, 735
- Williams, B. F., Naik, S., Garcia, M. R., & Callanan, P. J. 2006, *ApJ*, 643, 356

Zaritsky, D., Kennicutt, R. C., Jr., & Huchra, J. P. 1994, ApJ, 420, 87

Table 1: Log of stellar objects observed in the direction of M31.

M31								
Optical ID <sup>♠</sup> (Massey)	xID <sup>♣</sup> (Piestch)	RA (J2000)	Dec (J2000)	Offset arcsec	Offset $\sigma$	Date (yyyy-mm-dd)	Band <sup>♡</sup> (B,R)	Exposure (s per Band)
LGGS_J004123.75+411459.6	<b>136</b>	00 41 23.75	41 14 59.6	1.5	1.0	2008-10-26	B,R	3x2700
LGGS_J004130.37+410500.9	<b>146</b>	00 41 30.37	41 05 00.9	2.5	3.1	2006-10-23	B,R	4x900
LGGS_J004210.24+405149.4	<b>224a</b>	00 42 10.24	40 51 49.4	2.6	3.3	2007-10-10	B,R	3x2700
LGGS_J004210.38+405148.1	<b>224b</b>	00 42 10.38	40 51 48.1	0.7	0.9	2009-10-18	B,R	3x1800
LGGS_J003937.29+404925.8	<b>235-st</b>	00 39 37.3	40 49 25.8	4.8	2.6	2011-09-26	B,R	4x2700
LGGS_J003937.27+404928.9	<b>235-st</b>	00 39 37.3	40 49 28.9	2.6	1.4	2012-11-08	B,R	3x2400
LGGS_J004216.78+404814.4	<b>242</b>	00 42 16.78	40 48 14.4	2.3	3.1	2006-10-26	B,R	950,7x1200
						2006-10-29	B,R	3x1200
LGGS_J004218.72+411401.2	<b>246</b>	00 42 18.72	41 14 1.2	0.2	0.1	2006-11-16	B	1200,2x900
LGGS_J004231.23+410435.3	<b>278</b>	00 42 31.23	41 4 35.3	1.3	1.9	2007-08-11	B	5x1800
LGGS_J004259.07+413731.4	<b>367</b>	00 42 59.07	41 37 31.4	2.6	3.7	2008-09-23	B,R	1800,2x2700
LGGS_J004258.94+413727.3	<b>367obj1</b>	00 42 58.94	41 37 27.3	2.3	3.3	2009-10-18	B,R	3x1800
LGGS_J004309.86+411900.9	<b>405</b>	00 43 9.86	41 19 0.9	0.2	0.1	2009-07-24	B,R	3x1800
LGGS_J004310.50+413852.0	<b>407</b>	00 43 10.50	41 38 52.0	2.0	1.6	2008-09-26	B,R	5x1800
LGGS_J004333.64+411404.8	<b>466</b>	00 43 33.64	41 14 04.8	3.1	1.6	2007-10-09	B,R	2700,2x2500
LGGS_J004445.06+415153.4	<b>581</b>	00 44 45.06	41 51 53.4	1.4	0.8	2006-11-14	B	3x2700
LGGS_J004456.78+413548.0	<b>599</b>	00 44 56.78	41 35 48.0	0.1	0.1	2006-11-14	B	1800,3x2700
LGGS_J004506.46+420615.8	<b>612</b>	00 45 06.46	42 06 15.8	2.4	0.9	2006-11-16	B	3x2700
LGGS_J004513.59+413805.7	<b>620</b>	00 45 13.59	41 38 5.7	2.8	1.5	2008-09-23	B,R	3x2700
LGGS_J004604.83+415142.4	<b>705</b>	00 46 04.83	41 51 42.4	3.0	2.0	2007-11-03	B,R	5x1800
LGGS_J004557.04+414830.0	<b>1716-st</b>	00 45 57.04	41 48 30	1.1	1.1	2012-20-08	B,R	3x2400

♠ Optical source numbers from Massey et al. (2006)

♣ X-ray source numbers from PFH2005 (M31).

♡ B = blue (3750 - 5400Å), R = red (5200 - 8000Å)

<sup>1</sup> the spectrum is a composite of Massey sources LGGS\_J004353.35+411656.1, LGGS\_J004353.36+411656.1, LGGS\_J004353.37+411656.9, LGGS\_J004353 (see text)

Table 2: X-ray properties of stellar spectra from Table 1.

Object Name		Detection Likelihood		X-ray Properties						Class
[PFH 2005]	[Stiele 2011]	Chandra	LH	$f_X$ (mW/m <sup>2</sup> )	$f_X/f_{Opt}$	HR1	HR2	HR3	HR4	
	235		19.8	6.95(1.0) e-15		-	-	0.89(0.17)	-0.02(0.18)	<hard>
	1716		460	2.84(0.2) e-14		0.59(0.26)	0.71(0.07)	0.05(0.06)	-0.11(0.08)	<hard>
<b>136</b>	623		83	1.3(0.2) e-14		0.11(0.12)	-0.36(0.14)	-0.52(0.29)	-	<fg>
				1.03(0.22) e-14		0.29(0.14)	-0.27(0.16)	-0.74(0.28)	-	
<b>146</b>	-		9.3	2.6(0.8) e-15		0.97(0.18)	-0.26(0.22)	-0.25(0.34)	0.46(0.30)	SNR
<b>224</b>	811		7.5	2.4(0.8) e-15		-0.53(0.25)	-	-	-	<SSS>
				2.78(0.78)e-15		-0.46(0.46)	0.48(0.46)	-0.83(0.36)	-	<hard>
<b>242</b>	842		76	5.5(0.7) e-15		0.48(0.10)	-0.90(0.10)	-	-	<SNR>
				6.79(0.7)e-15		0.54(0.09)	-0.55(0.10)	-1.00(0.15)	-	< fg >
<b>246</b>	855	r3-44	54000	4.8(0.04) e-13		0.45(0.01)	0.32(0.01)	-0.17(0.01)	-0.39(0.01)	GIC
				4.21(0.37)e-13		0.51(0.01)	0.32(0.01)	-0.17(0.01)	-0.36(0.01)	GIC
<b>278</b>	925		1000	3.9(0.1) e-14		0.31(0.04)	-0.01(0.04)	-0.57(0.04)	-0.26(0.13)	<hard>
				2.49(0.15)e-14		0.23(0.06)	-0.02(0.06)	-0.59(0.07)	-0.33(0.22)	<hard>
<b>367</b>	1097		86	1.3(0.2) e-14		-	0.70(0.18)	-0.02(0.13)	-0.38(0.26)	<hard>
				1.17(0.14)e-14		0.86(0.36)	0.64(0.14)	0.04(0.11)	-0.48(0.20)	<hard>
<b>405</b>	1152	r3-16	14000	1.7(0.02)e-13		0.47(0.02)	0.25(0.01)	-0.29(0.01)	-0.39(02)	<XRB>
				1.44(0.22)e-13		0.49(0.02)	0.26(0.02)	-0.28(0.02)	-0.38(0.02)	<XRB>
<b>407</b>	1156		28	5.3(0.9) e-15		-	0.85(0.33)	0.29(0.17)	0.08(0.18)	<hard>
				4.77(0.94)e-15		-	0.98(0.32)	0.25(0.19)	0.10(0.19)	<SNR>
<b>466</b>	1257		36	5.9(0.8) e-15		-	0.59(0.17)	-0.18(0.13)	-0.27(0.23)	<hard>
				6.4(1.3) e-15		-	0.58(0.23)	-0.27(0.19)	-0.24(0.35)	<hard>
				3.91(0.06)e-13		0.49(0.02)	0.13(0.01)	-0.45(0.01)	-0.84(0.03)	<GIC<
<b>581</b>	1514		140	1.8(0.2) e-14		0.43(0.25)	0.55(0.10)	-0.16(0.09)	-0.50(0.18)	<hard>
				9.1(0.9) e-15		0.57(0.19)	0.49(0.10)	-0.23(0.09)	-0.51(0.18)	<hard>
<b>599</b>	-		9.9	3.5(0.9) e-15		0.02(37)	-	0.40(0.31)	0.34(0.26)	<hard>
<b>612</b>	1579		16	7.7(2.0) e-15		-	0.73(0.23)	-0.15(0.21)	-0.25(0.38)	<hard>
				9.7(1.2) e-15		0.73(0.27)	0.54(0.14)	-0.01(0.12)	-0.42(0.20)	<hard>

Object Name			Detection Likelihood	X-ray Properties					Class	
[PFH 2005]	[Stiele 2011]	Chandra	LH	$f_X$ (mW/m <sup>2</sup> )	$f_X/f_{Opt}$	HR1	HR2	HR3	HR4	
<b>620</b>	1598		25	8.4(1.0)e-15		0.90(0.22)	0.19(0.18)	-0.23(0.18)	0.05(0.33)	<hard>
				7.3(1.4)e-15		1.00(0.17)	0.09(0.21)	-0.09(0.20)	-0.03(0.34)	<hard>
				2.8(0.2) e-14		0.47(0.18)	0.63(0.07)	-0.05(0.07)	-0.03(0.10)	<hard>
<b>705</b>	1744		58	1.2(0.2) e-14		-	0.74(0.14)	-0.19(0.12)	-0.30(0.25)	<hard>
				2.49(0.17)e-14		0.71(0.31)	0.69(0.07)	-0.06(0.07)	-0.39(0.09)	<hard>

Table 3: Optical properties of the stellar objects of Table 1.

Object Name		Optical Properties								Infrared Properties			
oID (LGS)	xID (Piestch)	RA	Dec	V	B-V	U-B	V-R	R-I	Q	2 MASS	J	H	K
LGGS_J004123.75+411459.6	<b>136</b>	00 41 23.75	41 14 59.6	20.293(0.011)	1.862(0.031)	0.761(0.081)	1.469(0.012)	2.049(0.005)	-0.580	00412375+4114596	15.335(055)	14.865(076)	14.416(070)
LGGS_J004130.37+410500.9	<b>146</b>	00 41 30.37	41 05 00.9	18.499(0.052)	0.052(0.009)	-1.017(0.013)	0.377(0.016)	-0.052(0.013)	-1.054				
LGGS_J003937.29+404925.8	<b>235-st</b>	00 39 37.3	40 49 25.8	20.468(0.012)	0.064(0.016)	-0.876(0.012)	0.098(0.018)	0.086(0.014)	-0.922				
LGGS_J003937.27+404928.9	<b>235-st</b>	00 39 37.3	40 49 28.9	20.952(0.020)	0.207(0.024)	-0.688(0.018)	0.198(0.027)	0.271(0.018)	-0.83				
LGGS_J004557.04+414830.0	<b>1716-st</b>	00 45 57.04	41 48 30	20.017(0.009)	0.123(0.014)	-0.355(0.013)	0.133(0.013)	0.182(0.009)	-0.44				
LGGS_J004210.24+405149.4	<b>224a</b>	00 42 10.24	40 51 49.4	19.387(0.004)	0.264(0.005)	-0.682(0.005)	0.206(0.006)	0.219(0.004)	-0.872				
LGGS_J004210.38+405148.1	<b>224b</b>	00 42 10.38	40 51 47.4	21.461(0.019)	0.367(0.026)	0.199(0.026)	0.272(0.031)	0.291(0.023)					
LGGS_J004216.78+404814.4	<b>242</b>	00 42 16.78	40 48 14.4	19.419(0.004)	-0.104(0.005)	-0.993(0.004)	-0.013(0.006)	-0.010(0.005)	-0.918	00421645+4048113	16.381(117)	16.377:	15.151:
	<b>246</b>	00 42 18.72	41 14 1.2	18.260(0.055)	-0.238(0.078)	-1.809(131)	0.166(089)	-	-1.638	00421865+4114021	13.644(029)	13.158(034)	13.038(036)
LGGS_J004231.23+410435.3	<b>278</b>	00 42 31.23	41 4 35.3	19.935(0.005)	0.296(0.007)	-0.632(0.006)	0.299(0.008)	0.530(0.007)	-0.845				
LGGS_J004259.07+413731.4	<b>367</b>	00 42 59.07	41 37 31.4	20.127(0.008)	0.465(0.014)	-0.247(0.015)	0.368(0.011)	0.416(0.007)	-0.582	00425913+4137321	15.945(087)	15.087(097)	14.709(104)
LGGS_J004258.94+413727.3	<b>367obj1</b>	00 42 58.94	41 37 27.3	19.854(0.011)	0.757(0.021)	-0.647(0.025)	1.217(0.012)	1.401(0.005)	-1.192	00425892+4137273	15.505(0.0605)	14.641(0.071)	14.294(0.078)
LGGS_J004309.86+411900.9	<b>405</b>	00 43 9.86	41 19 0.9	18.098(0.014)	1.034(0.017)	0.819(0.017)	0.731(0.017)	0.644(0.010)	0.074	00430986+4119006	15.431(074)	14.597(075)	14.400(088)
LGGS_J004310.50+413852.0	<b>407</b>	00 43 10.50	41 38 52.0	19.957(0.008)	0.467(0.015)	-0.703(0.015)	0.268(0.012)	0.297(0.009)	-1.039				
LGGS_J004333.64+411404.8	<b>466</b>	00 43 33.64	41 14 04.8	19.495(0.004)	0.544(0.006)	-0.296(0.006)	0.337(0.006)	0.323(0.005)	-0.688				
LGGS_J004445.06+415153.4	<b>581</b>	00 44 45.06	41 51 53.4	20.623(0.011)	-0.118(0.016)	-0.963(0.013)	-0.019(0.018)	0.082(0.014)	-0.878				
LGGS_J004456.78+413548.0	<b>599</b>	00 44 56.78	41 35 48.0	20.534(0.011)	0.073(0.019)	-0.893(0.018)	0.196(0.017)	0.555(0.011)	-0.946				
LGGS_J004506.46+420615.8	<b>612</b>	00 45 06.46	42 06 15.8	20.771(0.013)	-0.064(0.018)	-1.088(0.014)	-0.022(0.022)	0.157(0.015)	-1.042				
LGGS_J004513.59+413805.7	<b>620</b>	00 45 13.59	41 38 5.7	19.932(0.007)	0.164(0.011)	0.121(0.012)	0.140(0.010)	0.242(0.007)	0.003				
LGGS_J004604.83+415142.4	<b>705</b>	00 46 04.83	41 51 42.4	18.145(0.004)	0.481(0.004)	-0.062(0.004)	0.328(0.004)	0.294(0.004)	-0.408	00460484+4151422	16.759(162)	16.855:	16.332:

Table 4: Set of Spectral Standard Stars for Cross-Correlation

Star	RA (J2000)	Dec. (J2000)	Spectral Type
HD188001	19:52.4	+18:40	O7.5 Iaf
B+60 447	02:11.7	+60:43	O9 Ia
B+61 154	00:43.3	+61:55	O9.5 V
B+57 153	00:49.0	+58:26	B0 V
B+63 33	00:21.8	+64:36	B1 V
B+58 351	02:00.7	+58:59	B1 III
B+60 191	01:14.5	+61:20	B2 IV
VOR+59 97	02:18.9	+59:59	B2 V
VOR+59	02:16.8	+59:46	B3 V
B+57 18	00:10.6	+58:45	B3 IV
B+57 58	00:19.9	+58:36	B5 V
L+60 221	02:10.5	+61:07	B5 III
HD13799	02:16.8	+62:57	B6 III
BSD 285	00:52.6	+59:41	B7 V
B+59 6	00:10.9	+60:26	B8 V
B+60 461	02:19.0	+61:09	B8 IV
LATT.161	00:44.7	+61:54	B9 V
B+59 35	00:20.4	+60:24	A0 V
B+60 51	00:26.6	+61:25	A2 IB
VOR+61 44	02:20.4	+61:56	A3 V
REB 149	01:56.6	+37:57	F5 V
BD+40349	01:41.8	+41:22	G0 V

Table 5: Most significant lines identified in the optical spectrum of [PFH2005] 146.

Red channel			
Element (wavelength)	Wavelength measured ( $\text{\AA}$ )	Flux ( $\text{erg s}^{-1}$ )	Vel. $\text{km s}^{-1}$
[NII] <b>5755</b>	5746.091	$(1.6 \pm 0.6) \times 10^{-15}$	–470
[NII] <b>6548</b>	6538.275	$(5.6 \pm 0.25) \times 10^{-14}$	–460
[NII] <b>6583</b>	6573.52	$(1.6 \pm 0.1) \times 10^{-13}$	–460
[H $\alpha$ ] <b>6563</b>	6552.952	$(3.5 \pm 0.2) \times 10^{-13}$	–460
[SII] <b>6716</b>	6706.437	$(5.6 \pm 0.2) \times 10^{-14}$	–450
[SII] <b>6731</b>	6720.711	$(4.8 \pm 0.2) \times 10^{-14}$	–450
Blue channel			
[H $\beta$ ] <b>4861</b>	4853.532	$(7.2 \pm 0.1) \times 10^{-14}$	–460
[OIII] <b>4959</b>	4950.453	$(6.8 \pm 0.4) \times 10^{-15}$	–510
[OIII] <b>5007</b>	4998.441	$(1.8 \pm 0.1) \times 10^{-14}$	–510

Table 6: Most significant Wolf-Rayet lines identified in the red optical spectrum of [PFH2005] 146.

Red channel			
Element (wavelength)	Wavelength measured ( $\text{\AA}$ )	Flux ( $\text{erg s}^{-1}$ )	Vel. $\text{km s}^{-1}$
[NII] <b>5755</b>	5746.091	...	–470
[NII] <b>6548</b>	6538.	$(1.4 \pm 0.1) \times 10^{-16}$	–460
[NII] <b>6583</b>	6574	$(5.7 \pm 0.2) \times 10^{-16}$	–410
[H $\alpha$ ] <b>6563</b>	6552.4	$(5.0 \pm 0.4) \times 10^{-16}$	–480
[SII] <b>6716</b>	6706.3	$(4.0 \pm 0.2) \times 10^{-16}$	–450
[SII] <b>6731</b>	6722.2	$(1.4 \pm 0.4) \times 10^{-16}$	–400
Blue channel			
[H $\beta$ ] <b>4861</b>	-	-	
[OIII] <b>4959</b>	4950.2	$(1.9 \pm 0.3) \times 10^{-16}$	–540
[OIII] <b>5007</b>	5000.3	$(3.5 \pm 0.1) \times 10^{-16}$	–420

Table 7: Most likely classification based on stellar spectra from Table 1.

Object Name	RA	DEC	Classification	Grade
<b>136</b>	00 41 23.75	41 14 59.6	Galactic Dwarf Nova	A
<b>146</b>	00 41 30.37	41 05 00.9	WN+O colliding winds	B
<b>224</b>	00 42 10.24	40 51 49.4	SNR	A
<b>235-st</b>	00 39 37.3	40 49 25.8	M31 HMXB	A
<b>242</b>	00 42 16.78	40 48 14.4	Galactic M star	B
<b>246</b>	00 42 18.72	41 14 1.2	M31 LMXB in GC	A
<b>278</b>	00 42 31.23	41 4 35.3	M31 HMXB	A
<b>367</b>	00 42 59.07	41 37 31.4	M31 HMXB	B
<b>405</b>	00 43 9.86	41 19 0.9	M31 symbiotic X-ray binary or LMXB	B
<b>407</b>	00 43 10.50	41 38 52.0	M31 BeXRB	A
<b>466</b>	00 43 33.64	41 14 04.8	M31 HMXB	B
<b>581</b>	00 44 45.06	41 51 53.4	Galactic CV	A
<b>599</b>	00 44 56.78	41 35 48.0	Bright source not counterpart	F
<b>612</b>	00 45 06.46	42 06 15.8	M31 HMXB	B
<b>620</b>	00 45 13.59	41 38 5.7	M31 HMXB	B
<b>705</b>	00 46 04.83	41 51 42.4	Bright source not counterpart	F
<b>1716-St</b>	00 45 57.04	41 48 30	M31 HMXB	B

Table 8: Radial Velocities of the M31 members, along with the radial velocity of the gas disc at their projected locations from the 21 cm map of Chemin et al. (2009).

Object Name	M31 HI R.V.	R.V. (km s <sup>-1</sup> )
146	-460	-450
224	-440	-450
235	-450	-250
246	-450	-350
278	-450	-400
367	-240	-350
405	-120	-180
407	-220	-140
466	-290	-130
612	-110	-110
620	-130	-160
1716	-120	-170

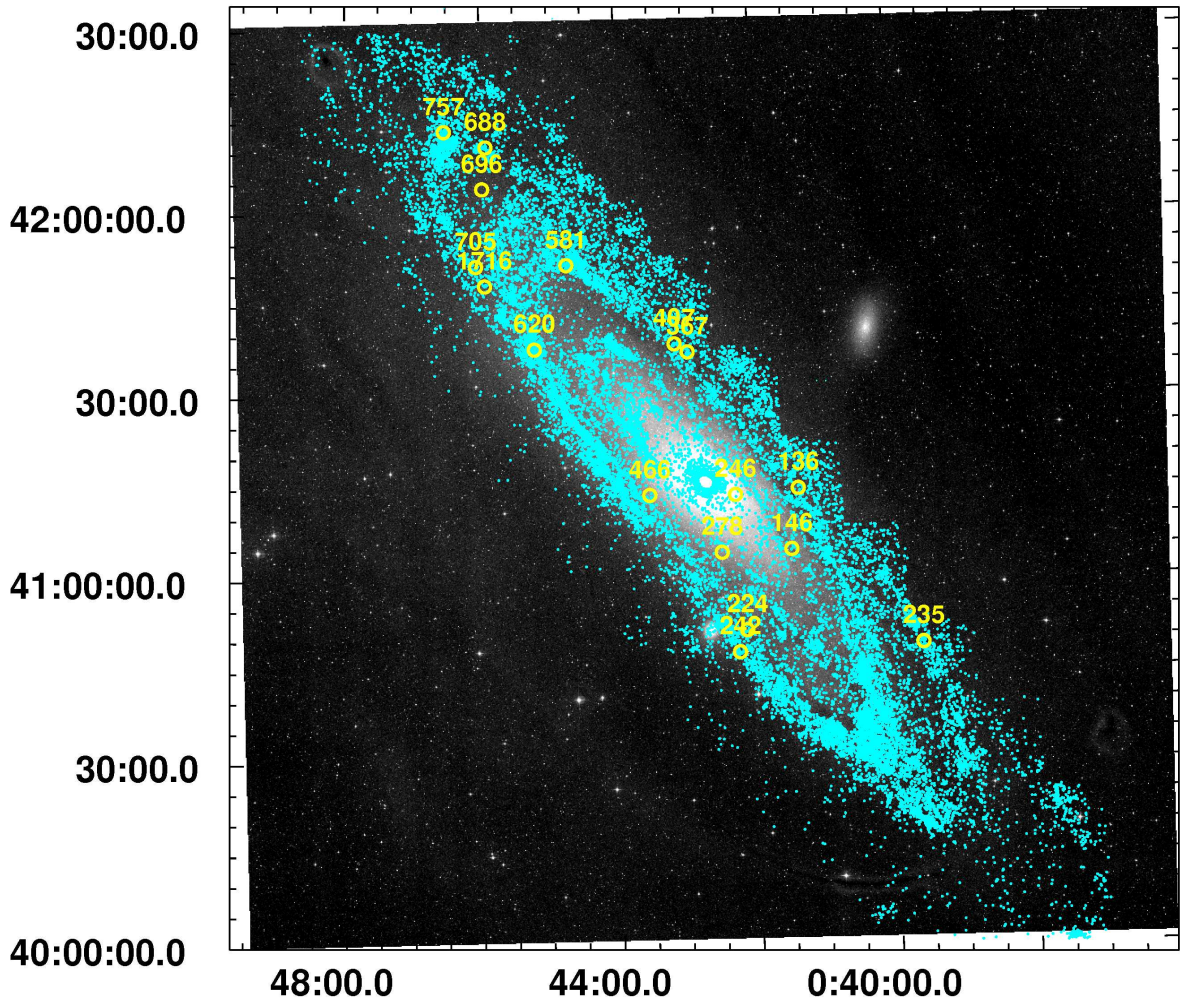


Fig. 1.— The location of the observed objects (yellow symbols) on an optical unfiltered image of M31 obtained with the Schmidt telescope on Calar Alto (using HDAP which was produced at Landessternwarte Heidelberg-Königstuhl under grant 00.071.2005 of the Klaus-Tschira-Foundation). The locations of OB stars in M31, delineating the spiral arms, are marked with cyan.

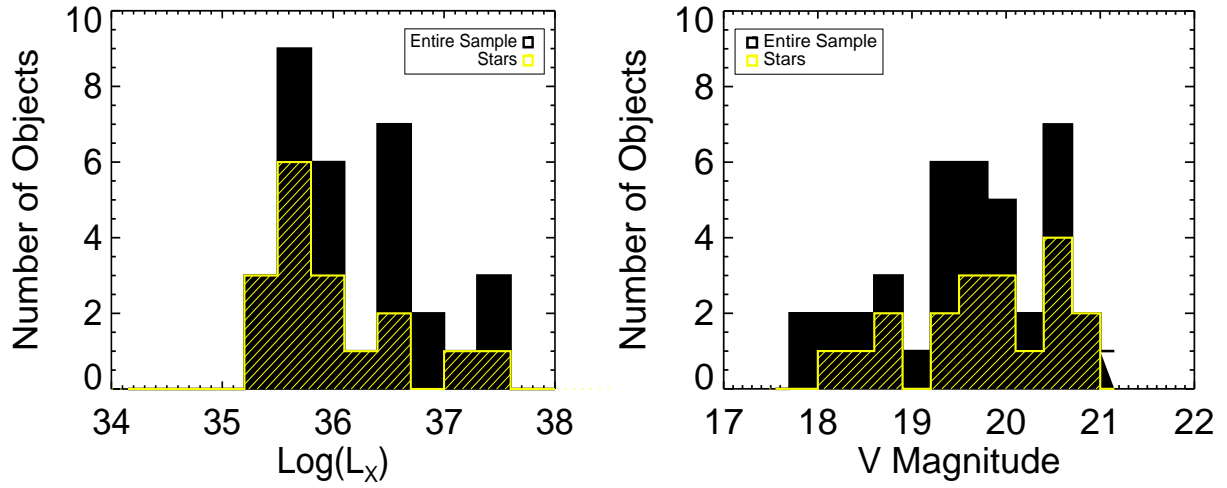


Fig. 2.— *Left:* Distribution of 0.2-4.5 keV X-ray luminosities (taking fluxes from Pietsch et al. (2005) and Stiele et al. (2011) and assuming they are at the distance of M31) for the sample of sources with optical counterpart candidates observed by our study (black), and those that we classified as stars (yellow). *Right:* Distribution of *V*-band magnitudes of the counterpart candidates observed for this study (black), and those that we classified as stars (yellow).

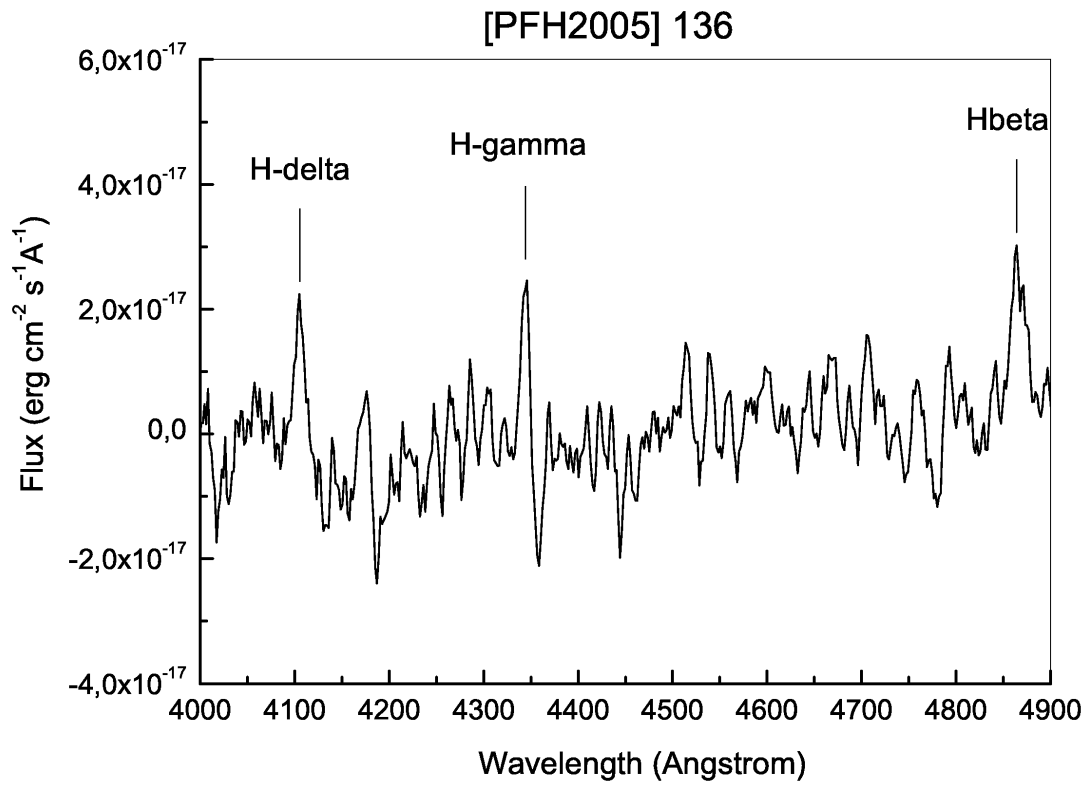


Fig. 3.— Blue spectrum of [PFH2005] M31\_136 showing Balmer line emission, expected in spectra of UGem variables when in quiescence.

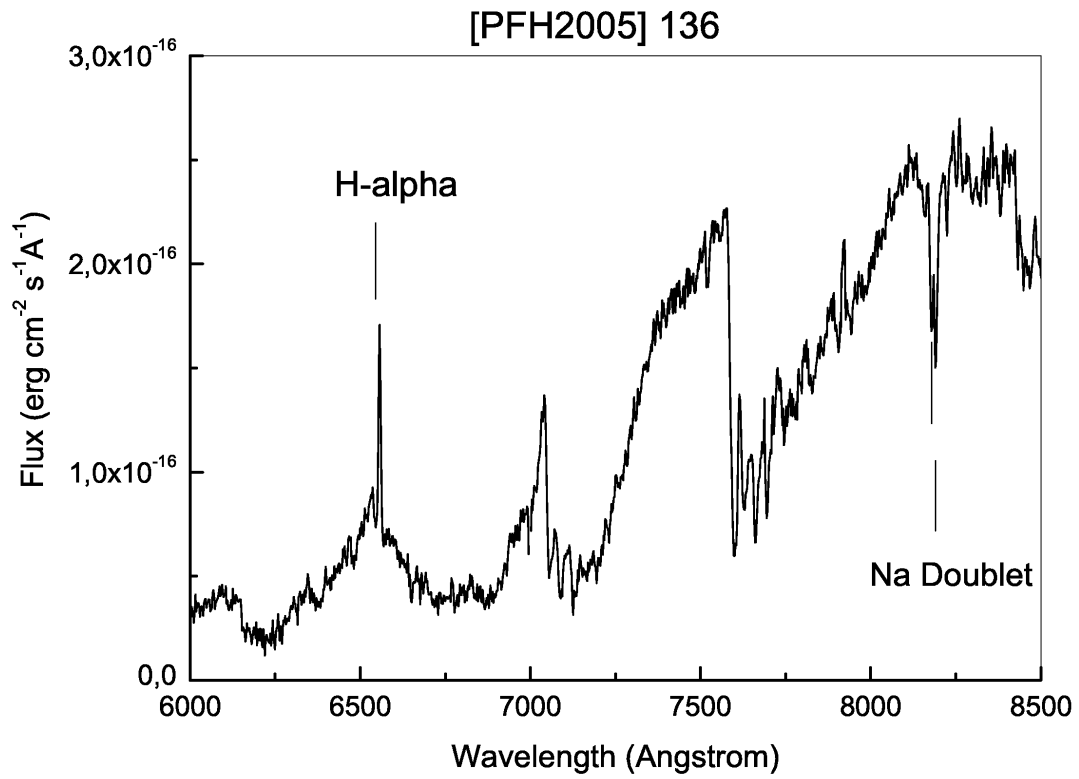


Fig. 4.— Red spectrum of [PFH2005] M31\_136 showing the characteristic features of an M5-6 dwarf, with H $\alpha$  emission.

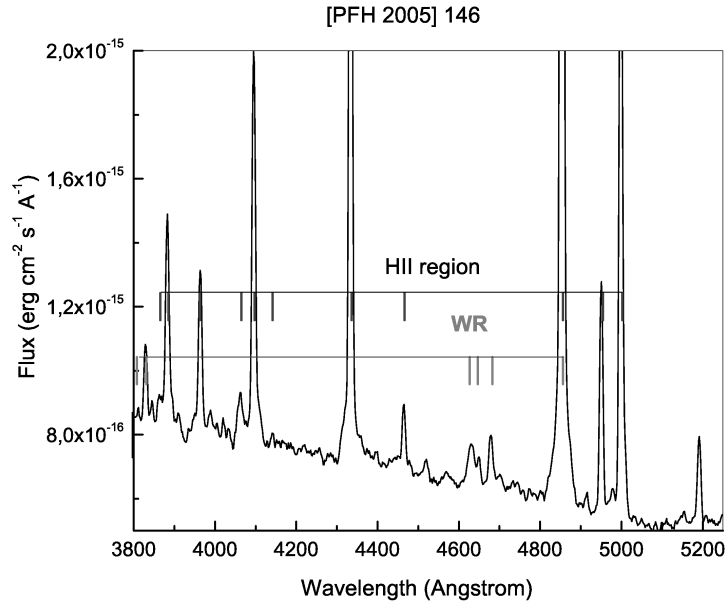


Fig. 5.— Blue part of the spectrum of [PFH2005] M31\_146 showing characteristic lines of a WN Wolf Rayet star embedded in an HII region.

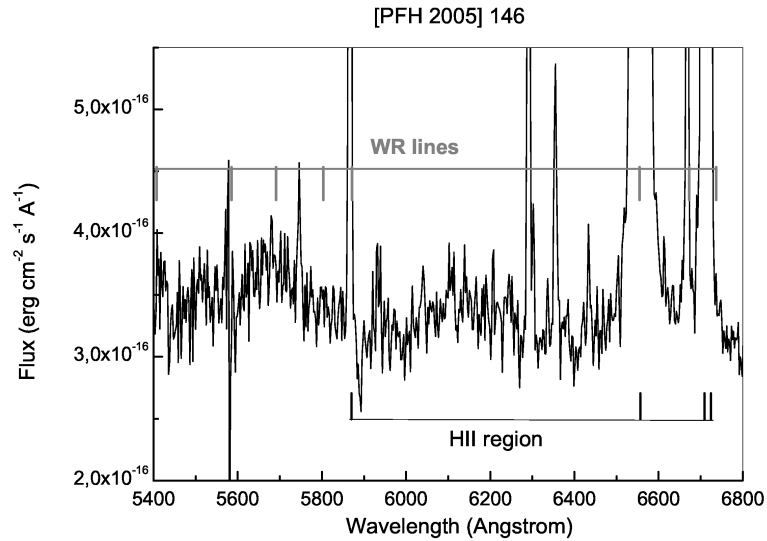


Fig. 6.— Red part of the spectrum of [PFH2005] M31\_146 showing characteristic lines of a WN Wolf Rayet star embedded in an HII region.

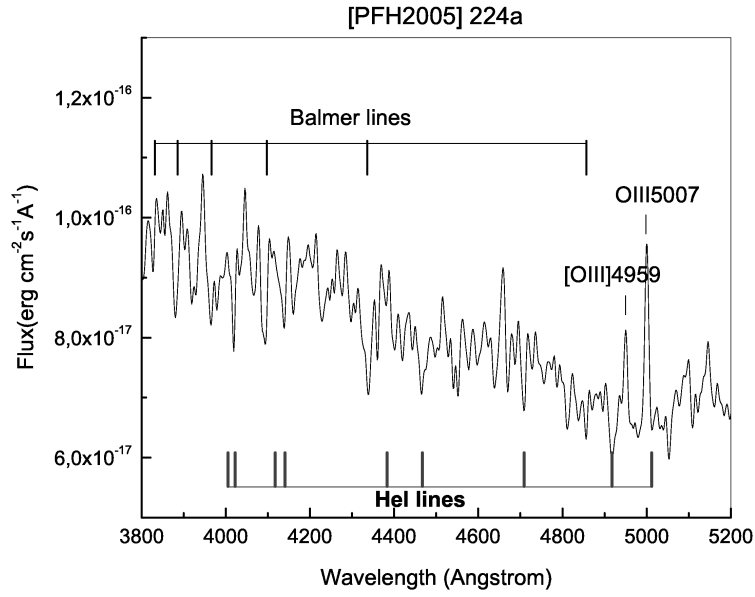


Fig. 7.— The blue part of the spectrum of [PFH2005] M31\_224a showing characteristic absorption lines of HeI and Hydrogen characteristic of an OB star.

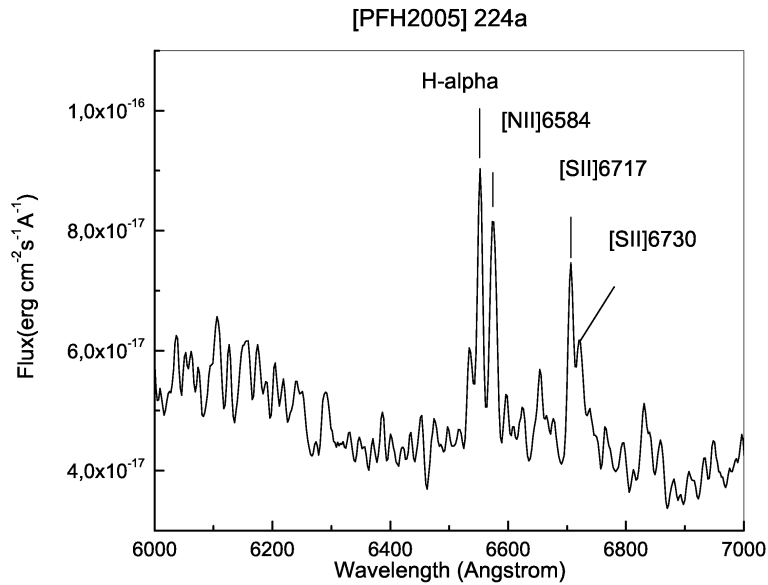


Fig. 8.— The red part of the spectrum of [PFH2005] M31\_224a showing characteristic emission lines of a SNR.

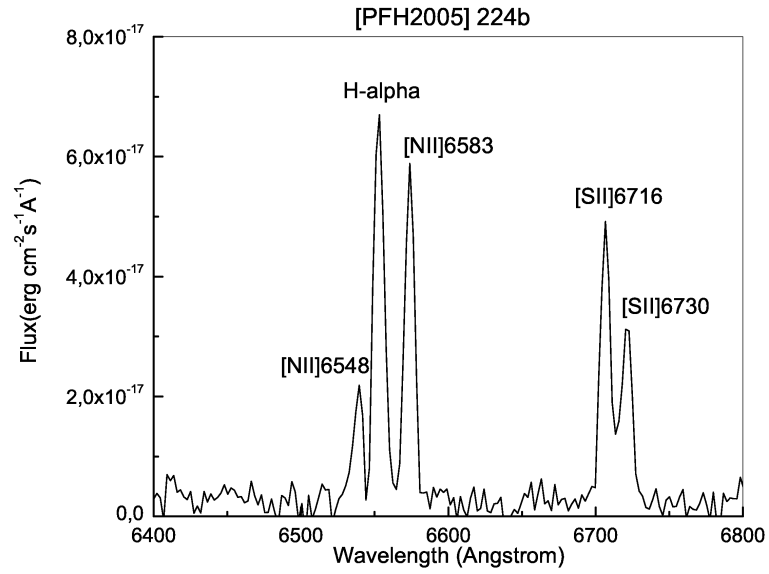


Fig. 9.— The red part of the spectrum of [PFH2005] M31\_224b showing characteristic emission lines of a SNR.

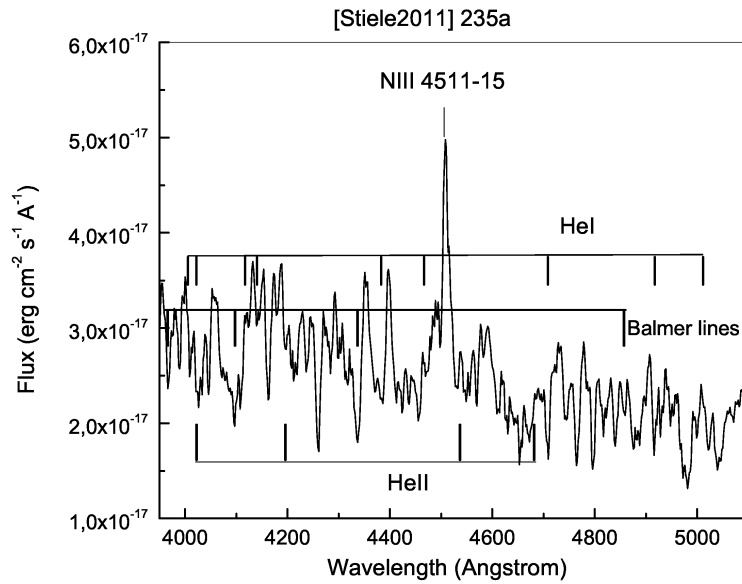


Fig. 10.— The blue part of the spectrum of [Stiele2011] M31\_235a showing characteristic emission of an O-type star.

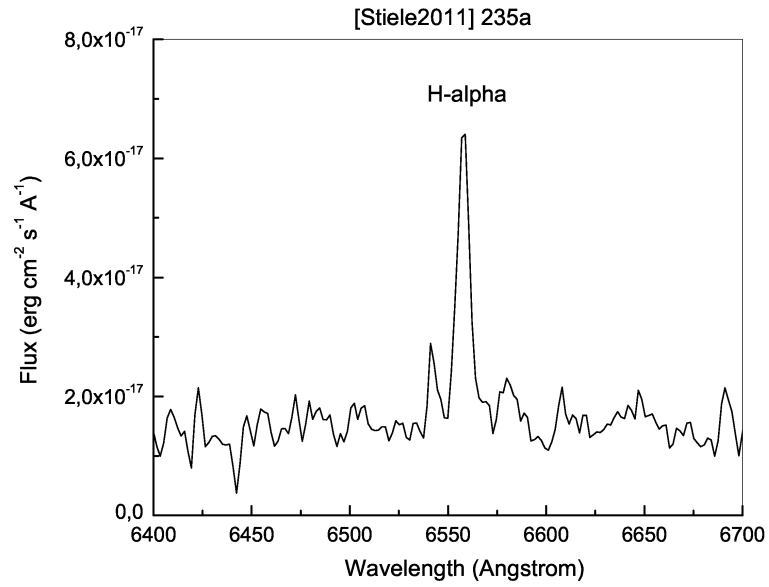


Fig. 11.— The red portion of the spectrum of [Stiele2011] M31\_235a showing a strong H $\alpha$  emission line.

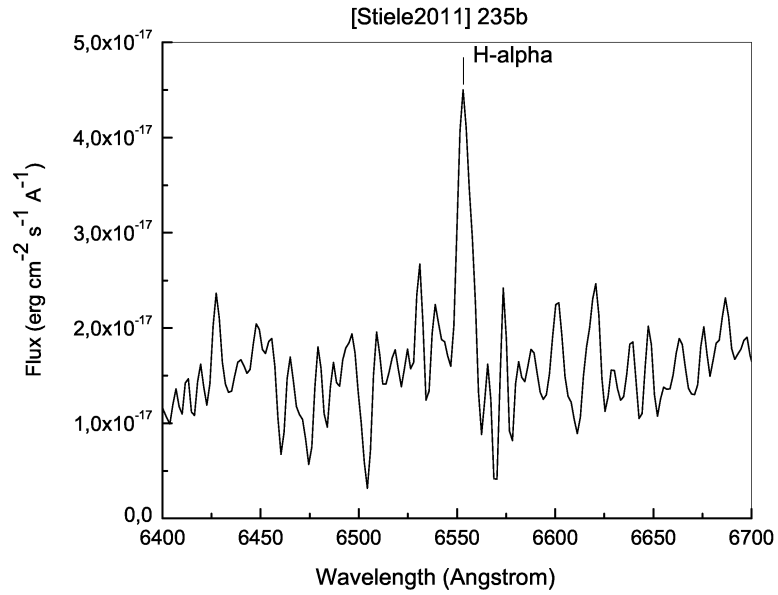


Fig. 12.— The red portion of the spectrum of [Stiele2011] M31\_235b showing H $\alpha$  in emission.

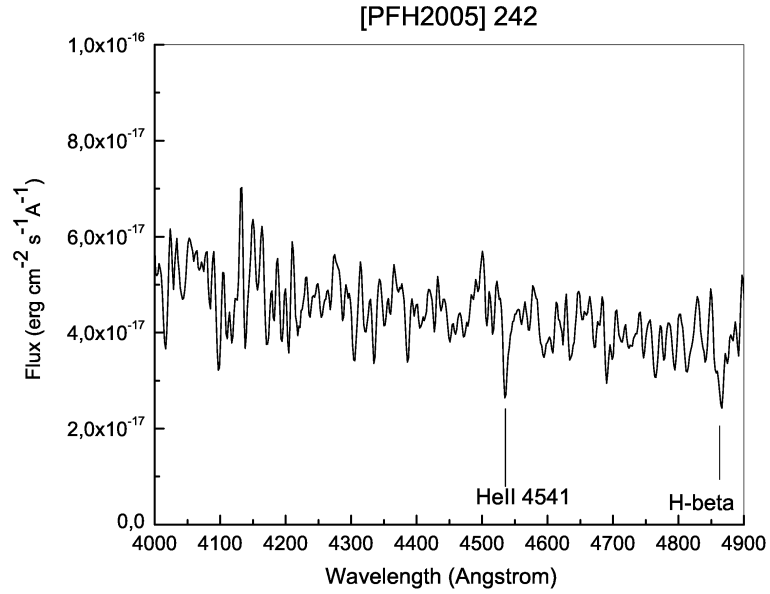


Fig. 13.— Blue spectrum of [PFH2005] M31\_242 showing possible HeII line

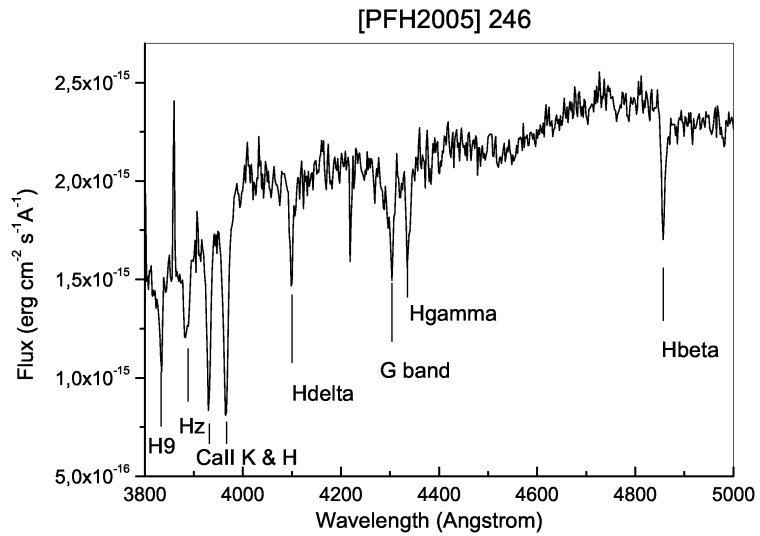


Fig. 14.— Blue part of the spectrum of [PFH2005] M31\_246. Composite spectrum of an old globular cluster.

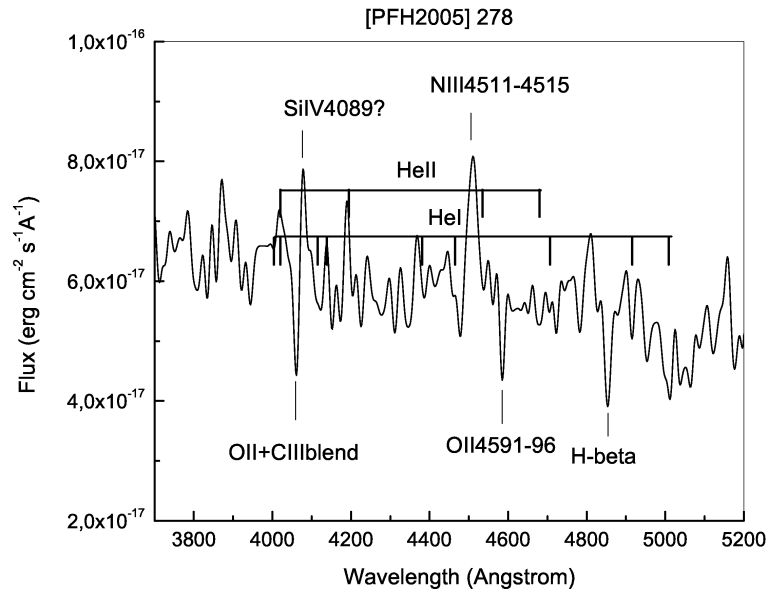


Fig. 15.— Part of the blue spectrum of the early type star (early B supergiant) which is the brightest candidate counterpart for M31\_278.

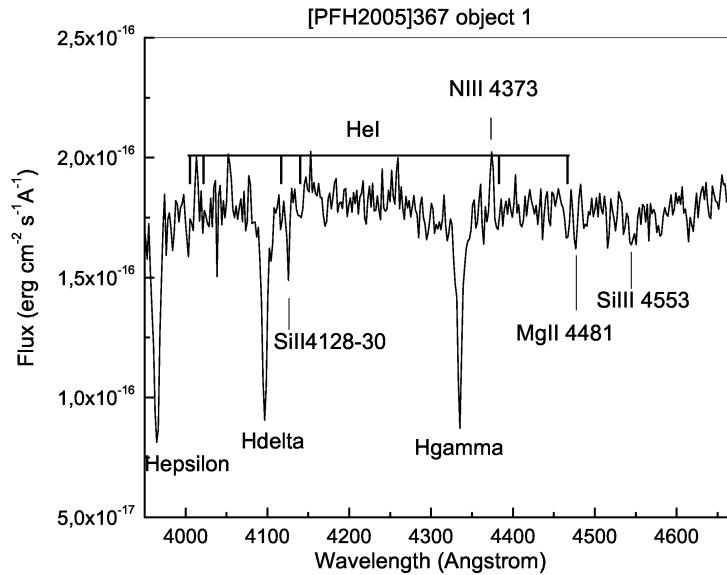


Fig. 16.— Part of the blue spectrum of the early type star which is the brightest candidate counterpart for M31\_367.

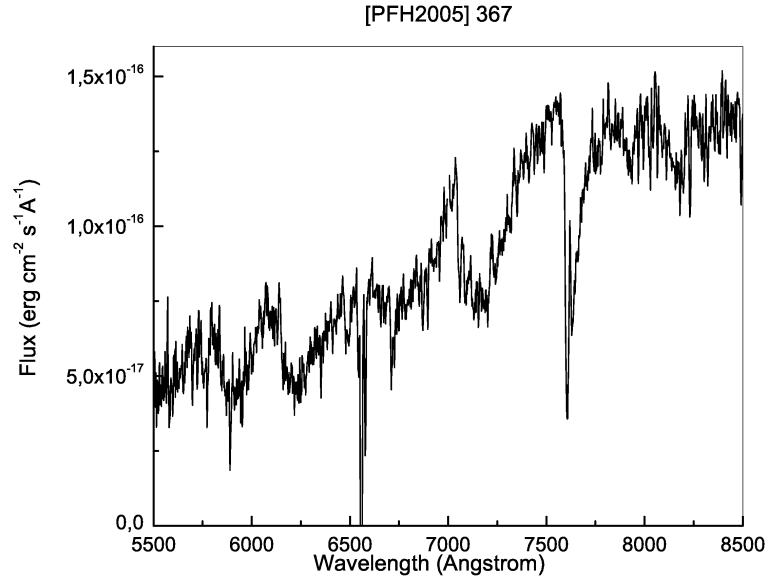


Fig. 17.— Part of the red spectrum of an M foreground star within the error circle of M31\_367.

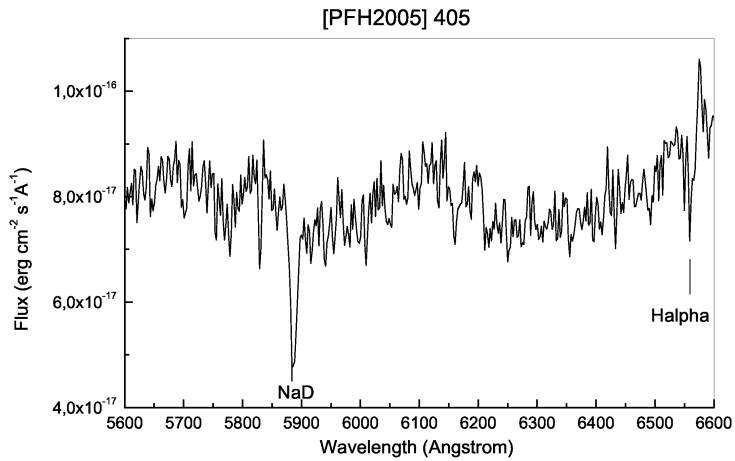


Fig. 18.— Part of the red spectrum of the optical counterpart of M31\_405, consistent with a K supergiant in M31.

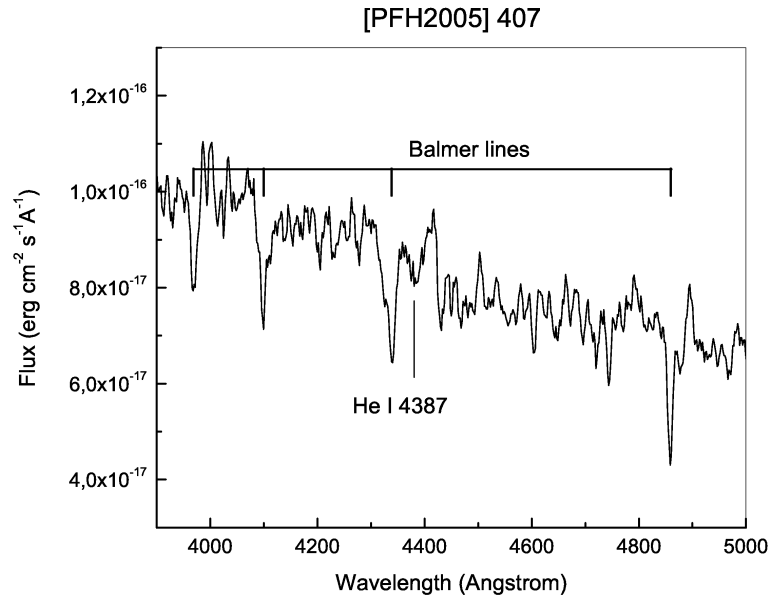


Fig. 19.— Blue part of the spectrum of the brightest optical counterpart of M31\_407, consistent with a B star in M31.

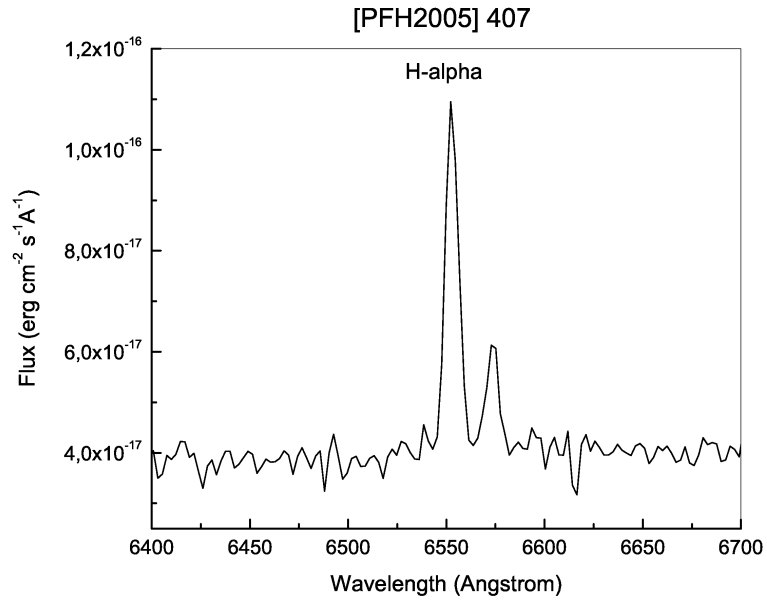


Fig. 20.— Red part of the spectrum of the brightest optical counterpart of M31\_407, showing H $\alpha$  emission.

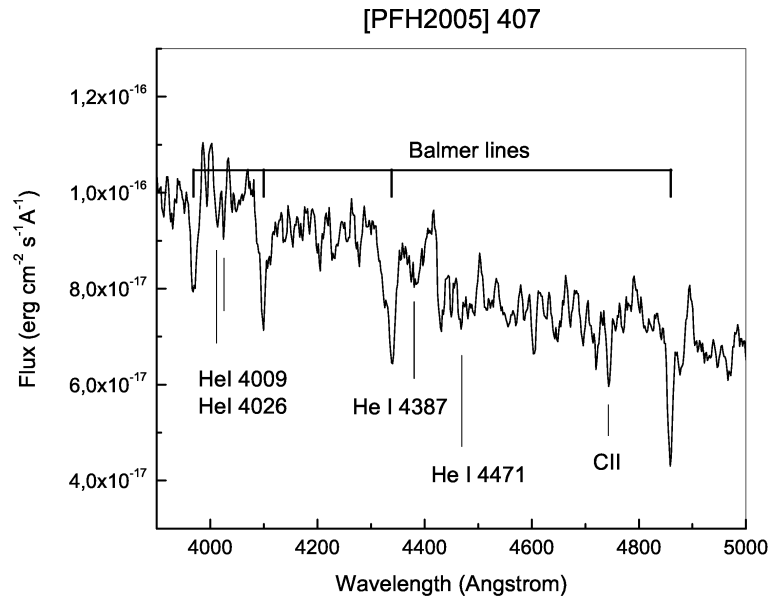


Fig. 21.— Blue part of the spectrum of the brightest optical counterpart of M31\_466, consistent with an O star in M31.

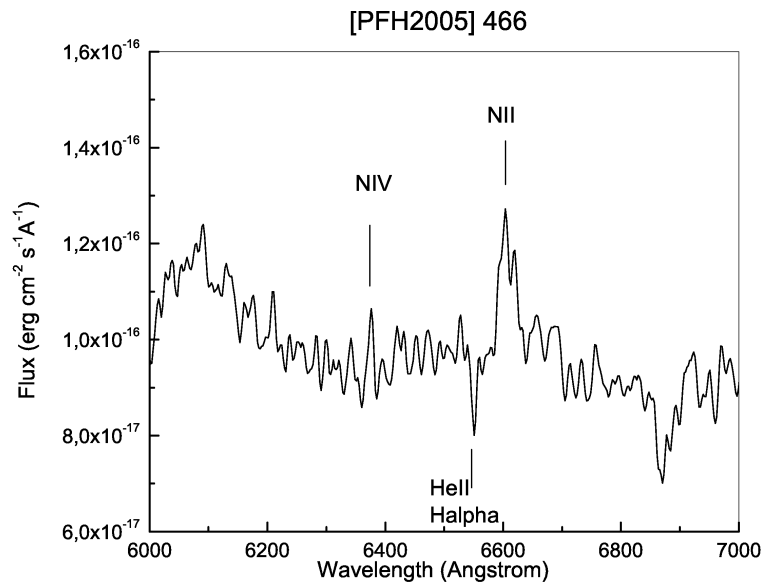


Fig. 22.— Red part of the spectrum of the brightest optical counterpart of M31\_466, showing clear NII emission, pointing to a late type O supergiant.

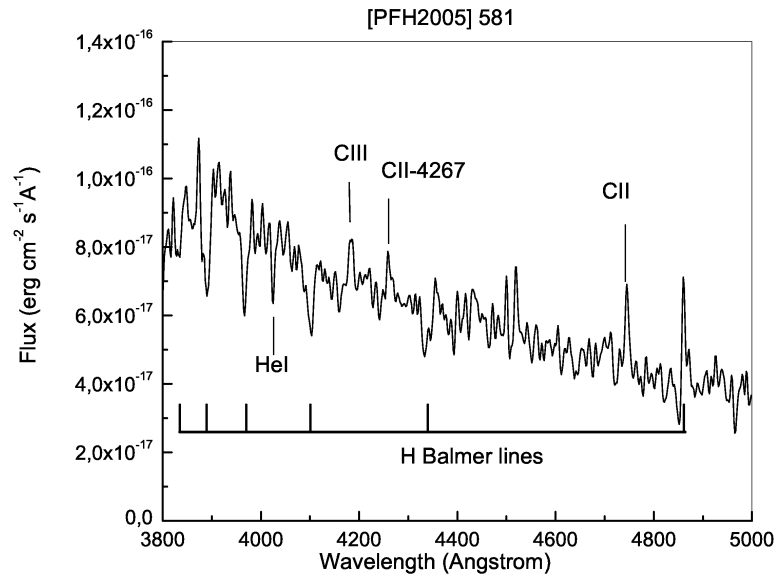


Fig. 23.— Blue part of the spectrum of the brightest optical counterpart of M31\_581, consistent with a Galactic cataclysmic variable star.

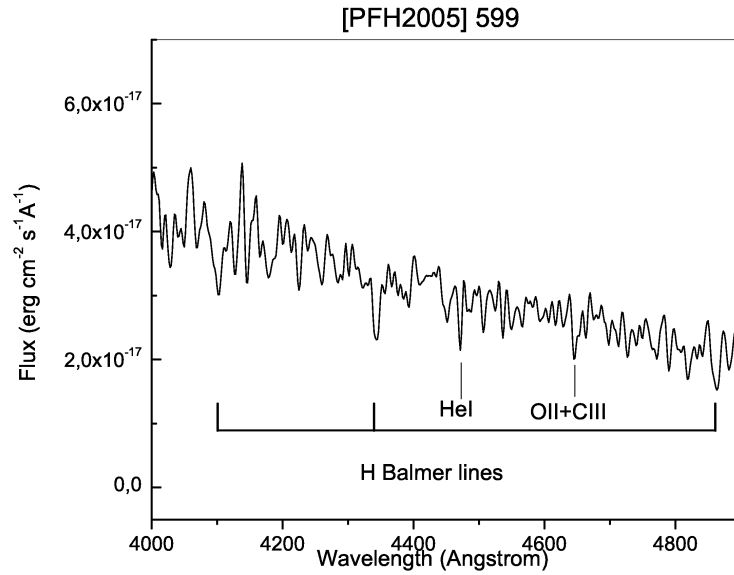


Fig. 24.— Blue part of the spectrum of the brightest optical counterpart of M31\_599, consistent with a Galactic early type star.

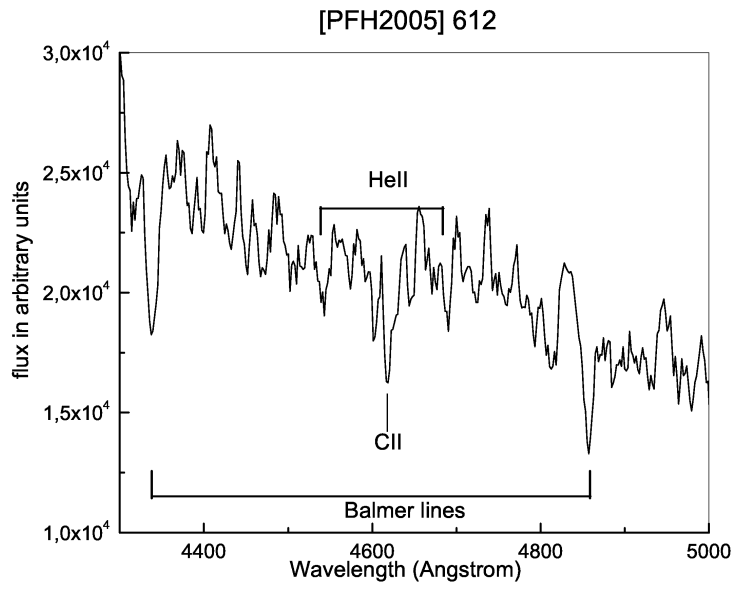


Fig. 25.— Part of the blue spectrum of [PFH2005] 612, characteristic of an early type star

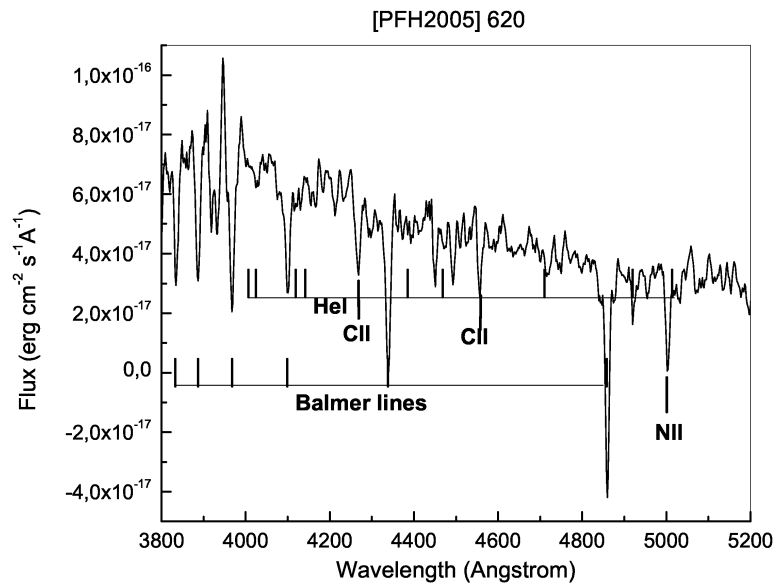


Fig. 26.— Part of the blue spectrum of [PFH2005] 620, showing an early type star.

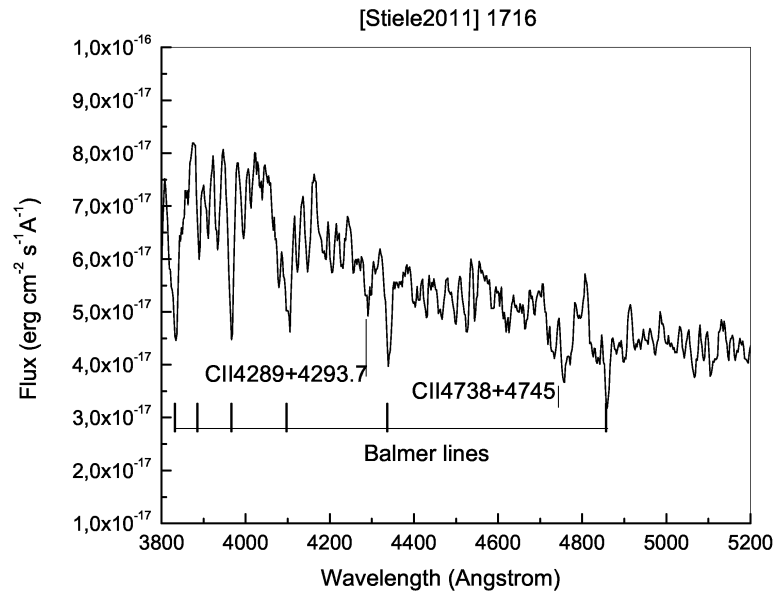


Fig. 27.— Part of the blue spectrum of [Stiele2011] M31\_1716, characteristic of a Be-type star.

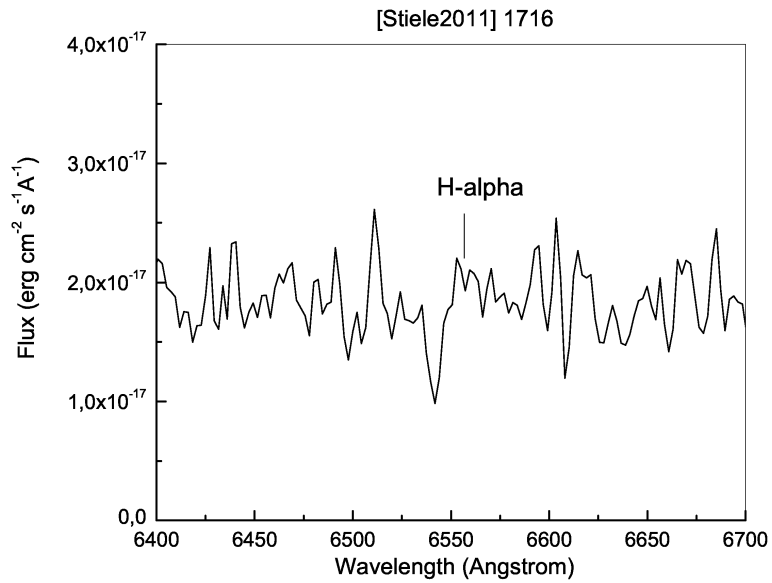


Fig. 28.— Part of the red spectrum of [Stiele2011] M31\_1716, showing the  $\text{H}\alpha$  line.

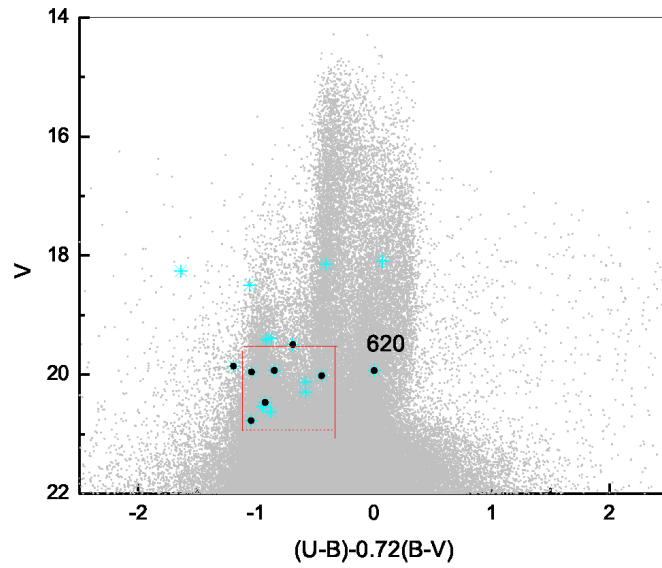


Fig. 29.— Colour-magnitude diagram of apparent magnitude vs. the reddening free Q-parameter  $Q=U - B - 0.72(B - V)$ , for all stars in the LGGs-M31 catalogue with both U-B and B-V colours measured (grey dots). Cyan bullets mark the location of all objects in the present study (according to Table 3). Black dots signify the subset of objects for which we have given a classification of a candidate HMXB of class A or B. The red box indicates the locus of BeXRBs in the SMC and the Galaxy moved to the distance of M31 (the faint limit is the observational limiting magnitude of our survey).

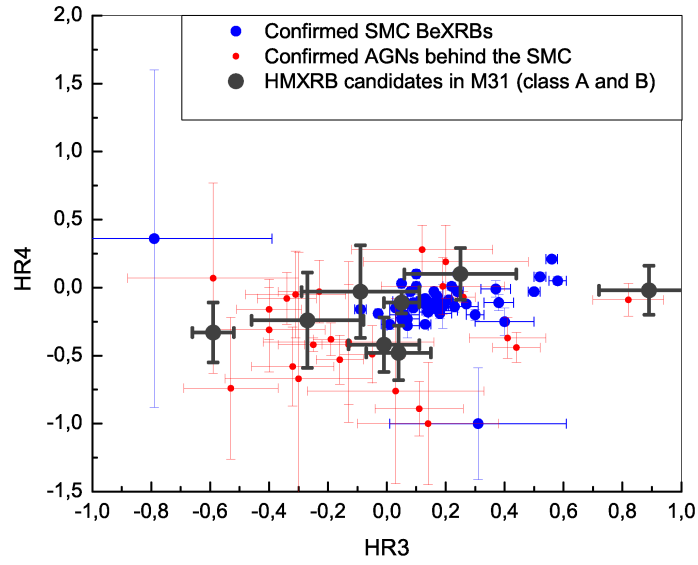


Fig. 30.— X-ray hardness ratio diagram, of HR4 versus HR3 (see Table 2. Blue dots mark confirmed BeXRBs in the Small Magellanic Cloud (SMC). Red dots mark confirmed AGNs behind the SMC, from (Sturm et al. 2013). Grey shows class A and class B HMXB candidates from Table 7 (see Section 4).